DOI:
10.1038/s41591-018-0102-y

Document Version
Peer reviewed version

Cold-induced epigenetic programming of the sperm enhances brown adipose tissue activity in the offspring

Authors:
Wenfei Sun[1†], Hua Dong[1†], Anton S. Becker[1,3,4], Dianne Helerie Dapito[1], , Salvatore Modica[1], Gerald Grandl[1], Lennart Opitz[1,2], Vissarion Efthymiou[1], Leon Gabriel Straub[1], Gitalee Sarker[1], Miroslav Balaz[1], Lucia Balazova[1], Aliki Perdikari[1], Elke Kiehlmann[1], Sara Bacanovic[4], Caroline Zellweger[4], Daria Peleg-Raibstein[1], Pawel Pelczar[5], Wolf Reik[6,7], Irene A. Burger[4], Ferdinand von Meyenn[6,8], Christian Wolfrum[1*]

Affiliations:
[1]Institute of Food, Nutrition and Health, ETH Zurich, Schwerzenbach, Switzerland
[2]Functional Genomics Center Zurich, ETH Zurich/University of Zurich, Zurich, Switzerland
[3]Institute of Diagnostic and Interventional Radiology, University Hospital of Zurich, Zurich, Switzerland
[4]Clinic of Nuclear Medicine, University Hospital of Zurich, Zurich, Switzerland
[5]Center for Transgenic Models, University of Basel, Basel, Switzerland
[6]Epigenetics Programme, Babraham Institute, Cambridge, United Kingdom
[7]Wellcome Trust Sanger Institute, Hinxton, United Kingdom.
[8]Department of Medical & Molecular Genetics, King's College London, London, UK

[*]Correspondence to:

Swiss Federal Institute of Technology
Department of Health Sciences and Technology
CH-8603 Schwerzenbach
christian-wolfrum@ethz.ch

[†]These authors contributed equally to this work.

Key Words

Metabolic syndromes; Obesity; Brown adipose tissue; Transgenerational regulation

Abstract

Recent research has focused on environmental effects controlling tissue functionality and systemic metabolism. However, whether such stimuli affect human thermogenesis and body-mass index (BMI) has not been explored. Here, we show retrospectively that the presence of brown adipose tissue (BAT) and the season of conception are linked to BMI in humans. In mice, we demonstrate that cold exposure of males, but not females, before mating results in improved systemic metabolism and protection from diet induced obesity of the male offspring. Integrated analyses of the DNA methylome and RNA-seq of the sperm from male mice reveal several clusters of co-regulated differentially methylated regions (DMR) and differentially expressed genes (DEG), suggesting that the improved metabolic health of the offspring is due to enhanced BAT formation and increased neurogenesis. The conclusions are supported by cell-autonomous studies in the offspring demonstrating an enhanced capacity to form mature active brown adipocytes, improved neuronal density and more norepinephrine release in BAT in response to cold stimulation. Taken together, our results indicate that in humans and in mice seasonal or experimental cold exposure induces an epigenetic programming of the sperm such that the offspring harbor hyper-active BAT and an improved adaptation to overnutrition and hypothermia.

Introduction

In 2016, 39% of all adults worldwide were classified as overweight (BMI >25) and 13% as clinically obese (BMI >30) (ref. 1). This imposes a burden on society as obesity-associated co-morbidities, linked to an increase in adipose tissue mass, are the main contributors to overall mortality and health care costs. Adipose tissue functions as a

dynamic endocrine organ[2] and therefore its "quality" is considered to be an important factor in the development of obesity associated co-morbidities[3]. Adipose tissue can be divided into the functionally and morphologically distinct white (WAT) and brown adipose tissues (BAT)[4]. The main function of BAT is energy dissipation via non-shivering thermogenesis[5], enabled by the presence of uncoupling protein 1 (UCP1) in the inner mitochondrial membrane. Thus, brown adipocytes contribute to the maintenance of body temperature during acute and chronic cold exposure[2,6].

Besides classical BAT found in rodents in the interscapular area (iBAT), a second type of thermogenic active fat cell (termed beige or brite adipocytes) has been described which is induced by cold exposure mainly in inguinal WAT (ingWAT)[7]. Analysis of ^{18}F-Fluorodeoxyglucose (FDG)-PET/CT scans demonstrated the presence of active BAT in adult humans, in supraclavicular, paravertebral and deep neck regions[8-13] and human BAT can be activated by mild cold exposure or by administration of a specific adrenergic receptor beta 3 (ADRB3)-agonist[14,15]. The relevance of BAT for physiology was inferred by the association with various metabolic parameters[15] and it was demonstrated that people with functional BAT can effectively lose weight by a mild cold stimulation regime[16].

In recent years, studies have demonstrated a link between paternal preconception nutrient exposure and the phenotype of the offspring[17,18]. Differences in gene expression patterns arise during development and can be retained through mitosis by epigenetic mechanisms[19]. In the context of thermoregulation, it was shown that environmentally-induced changes in gene expression can affect cellular function and thereby also the predisposition to certain diseases[20]. Additionally, changes in the environment can be transmitted to subsequent generations[18,21,22]. More specifically,

there have been indications that the season of birth and adult BMI show some correlation[23]. Here we studied the influence of environmental temperature and its effect on systemic metabolism, as well as the contribution of different thermogenic pathways using human and mouse studies.

Cold exposure before conception and during gestation activates brown and brite adipose tissue

To identify a possible correlation between ambient temperature and BAT abundance, we performed a retrospective study of FDG-PET/CT scans from 2007 – 2015 collected from the University Hospital of Zurich (*n* = 8440 individuals). Representative PET images from two individuals are shown in **Supplementary Fig. 1a**. Individuals with active BAT were 3.2% more likely to have been conceived in the colder period of the year, e.g. between October and February (mean temperature estimate 2 °C), while individuals without active BAT were more likely conceived in the warmer months, e.g. between April and September (mean temperature estimate 13 °C) (**Fig. 1a**). No apparent fluctuations in age (**Supplementary Fig. 1b**) or BMI (**Supplementary Fig. 1c**) were observed and the pattern persisted for different BAT activation strengths (**Supplementary Fig. 1d**). Among individuals conceived in the colder period (*n* = 3793), BAT positive individuals (*n* = 235) had a significantly lower BMI (mean 20.9 vs. 22.8; $p<0.001$) compared to age- and sex-matched BAT-negative individuals (**Fig. 1b**). These data identify a correlation between the season of conception and the propensity to form active BAT; however, given the retrospective nature and the large number of potential confounders, causality cannot be inferred. Hence, we investigated the effect of cold exposure (CE) before and during conception using mouse model systems. We analyzed offspring groups whose

parents had not been exposed to cold (23 °C) (Gp. 1) and those who had been exposed to cold (8 °C), either before conception (Gp. 2), before conception and during the first week of gestation (Gp. 3) or before conception and during week one and two of gestation (Gp. 4) (**Fig. 1c**). Interestingly, we observed that offspring from parents that were exposed to cold before conception showed higher UCP1 expression both in iBAT and in ingWAT under regular housing conditions (RT) (**Fig. 1d**). When we challenged offspring by CE, the effect on UCP1 expression was markedly enhanced (**Fig. 1e** and **Supplementary Fig. 1e**). Taken together, our data indicate that CE of parents before conception or during gestation results in higher basal and stimulated UCP1 expression in the iBAT and ingWAT of the offspring.

The effects of pre-conception cold exposure are mediated through the paternal lineage

Based on these findings, we analyzed whether the observed effect of CE was transmitted through the paternal (P-CE) or maternal (M-CE) lineage, focusing on the preconception exposure model in all subsequent studies. Intriguingly, we observed that the effects of parental CE on UCP1 expression at RT were mediated by the paternal lineage (**Fig. 2a**) and that the effect was enhanced in male iBAT and ingWAT and in female iBAT offspring when stimulated by CE (**Fig. 2b** and **Supplementary Fig. 2a**). Also, we could show that offspring from P-CE had higher UCP1 protein level than control (Ctrl) males at 21 days of age at RT and under thermoneutral (TN) conditions (**Supplementary Fig. 2b**,**c**). Analysis of gene expression in iBAT of P-CE offspring demonstrated higher mRNA expression of several markers of brown fat function in iBAT (**Fig. 2c**). We did not observe any changes in litter size and in nursing percentage over

the postnatal period (**Supplementary Fig. 2d**,**e**), suggesting that alterations in maternal behavior are not the cause for the observed phenotype. To exclude paternal behavior as a confounding factor, we performed *in vitro* fertilization (IVF) with sperm derived from P-CE or Ctrl males. We observed an induction of brown fat marker expression (**Supplementary Fig. 2f**) and UCP1 protein (**Fig. 2d** and **Supplementary Fig. 2g**) in iBAT of male and female P-CE vs Ctrl offspring, paralleled by a difference in body surface temperature (**Supplementary Fig. 2h**).

Since brown fat is formed at day E15.5 (ref. 24), we analyzed whether the observed changes were already present before birth. We could show that in iBAT from E18.5 embryos, *Ucp1* mRNA and other brown fat markers were higher (**Supplementary Fig. 2i**). Interestingly, these changes did not translate into an altered birth weight, nor did we observe differences in postnatal weight gain (**Supplementary Fig. 2j**). However, iBAT weight in 7-week old animals was significantly higher (**Supplementary Fig. 2k**), suggesting that not only expression of UCP1, but also the formation of iBAT is enhanced in P-CE offspring. In line with this, we could show by immunohistochemical analysis of iBAT and ingWAT that the area of $UCP1^+$ patches, denoting cells with high levels of UCP1 expression, was higher at RT in both iBAT and ingWAT (**Fig. 2e**,**f**). Upon CE, this phenotype was enhanced in both iBAT and ingWAT (**Fig. 2g**,**h**). We also observed lower lipid droplet size in ingWAT of P-CE offspring, suggesting a more active lipid metabolism (**Supplementary Fig. 2l**). Furthermore, reduced adipocyte size and more $UCP1^+$ cells were observed in P-CE offspring at 21 days of age at RT or at TN (**Supplementary Fig. 2m**-**o**). Taken together, our data demonstrate that the effect of CE is mediated through the paternal lineage and affects both UCP1 expression and adipose tissue morphology.

P-CE induces iBAT activity and systemic metabolism in the offspring

Based on these findings, we analyzed whether the effect of P-CE would translate into a higher thermogenic activity. Surface temperature was higher in P-CE offspring compared to Ctrl offspring at P7 (**Fig. 3a**) at RT. At 7 weeks of age, animals had the same body weight (**Supplementary Fig. 3a**) and the same surface temperature (**Fig. 3b**) at RT while upon CE, P-CE offspring exhibited a higher surface temperature (**Fig. 3b**). Furthermore, we observed that P-CE-derived offspring had an 11% higher VO_2 and VCO_2 at RT, which was enhanced upon acute CE (**Fig. 3c** and **Supplementary Fig. 3b**), while respiratory exchange ratio (RER) remained unchanged (**Supplementary Fig. 3c**). As CE can lead to shivering, we quantified the induction of brown fat in response to an i.p. injection of ADRB3-agonist CL316,243 (CL). We observed higher UCP1 protein (**Fig. 3d**), higher VO_2 and VCO_2 levels (**Fig. 3e** and **Supplementary Fig. 3d**), concomitant with more $UCP1^+$ cells in iBAT (**Fig. 3f**) of P-CE mice. Of special interest, we could show a lower RER in P-CE offspring following CL injection, suggesting a preferred utilization of fatty acids (**Supplementary Fig. 3e**).

Based on these data we analyzed whether the changes in respiration could lead to altered systemic metabolism. We did not observe any changes in body weight between 7 and 18 weeks of age (**Supplementary Fig. 3f**) when P-CE and Ctrl offspring were fed a regular chow diet at RT. Similarly, we did not observe any change in food intake (**Supplementary Fig. 3g**), however we could show that P-CE offspring exhibited a significant reduction in basal glucose levels as well as a trend for improved insulin sensitivity (**Supplementary Fig. 3h**). Insulin, cholesterol and fibroblast growth factor 21 (FGF21) levels were the same (**Supplementary Fig. 3i**-**k**), and P-CE offspring showed lower circulating triacylglycerol (TAG) levels (**Supplementary Fig. 3l**) and higher

circulating non-esterified fatty acids (NEFAs) under fasted conditions (**Fig. 3g**). To assess whether the changes in altered glucose homeostasis could be due to a higher glucose uptake into iBAT, we injected Ctrl and P-CE offspring at RT or after CE with radiolabeled 2-deoxy-glucose. We observed higher glucose uptake exclusively into iBAT and ingWAT of P-CE offspring while muscle, brain, liver and heart glucose uptake was not affected (**Fig. 3h** and **Supplementary Fig. 3m**). These changes were paralleled by an induction of facilitated glucose transporter member 4 (GLUT4) expression in iBAT under CE (**Fig. 3i**). Taken together, our data demonstrate that P-CE induces brown and brite adipocyte function in the offspring, which leads to an improved systemic metabolism.

The effect of P-CE is mediated in part through brown and brite adipocytes

As several tissues contribute to the maintenance of body temperature, we next aimed to assess the contribution of brown and brite adipocytes. Therefore, we employed a transgenic mouse line, which expresses a diphtheria toxin receptor (DTR)- green fluorescent protein (GFP) fusion protein under the control of the *Ucp1* promoter (Ucp1-DTR-GFP mice)[25]. Sequential injections of diphtheria toxin A (DTA) in these mice leads to the complete ablation of brown adipocytes, indicated by the reduction in iBAT mass (**Fig. 4a**) and loss of UCP1 protein expression in iBAT (**Fig. 4b**,**c**). Similar to P-CE wild type mice, P-CE offspring from the Ucp1-DTR-GFP line exhibited slightly higher VO_2 and VCO_2 at RT and a significant induction of both parameters upon CE at time point I (TP I) (**Fig. 4d** and **Supplementary Fig. 4a, TP I**). When mice were treated with DTA (TP II-IV), we observed a reduction in VO_2 and VCO_2 exclusively in P-CE offspring (**Fig. 4d** and **Supplementary Fig. 4a, TP II-IV**) which, after three consecutive injections of

DTA, led to the abrogation of the difference in VO_2 and VCO_2. The RER was not altered between the two groups at any time point (**Supplementary Fig. 4b**).

To avoid a shivering response in mice that received DTA injections, we analyzed respiration in animals in response to CL injections. We observed higher VO_2 and VCO_2 in P-CE vs. Ctrl offspring of Ucp1-DTR-GFP mice after CL treatment (**Fig. 4e** and **Supplementary Fig. 4c, TP I**). As the CL injections caused only a transient increase in respiration, we treated the animals by three subsequent injections with CL and DTA (**Fig. 4e** and **Supplementary Fig. 4c, TP II-IV**). Already after two injections with DTA the difference between P-CE and Ctrl offspring on both VO_2 and VCO_2 was lost, suggesting that brown and brite adipocytes might be in part responsible for the observed higher respiration in P-CE-derived offspring. Similarly, we observed a lower RER in P-CE-derived offspring after CL injection, which was lost after DTA injection (**Supplementary Fig. 4d**). These findings were supported by the observation that 24 hours after the third CL+DTA injection, we did not observe any difference in respiration between both groups (**Fig. 4f** and **Supplementary Fig. 4e**,**f**). To analyze whether the observed effects would also translate into an induction of thermogenesis, we quantified surface temperature after an injection of either CL, with or without DTA mediated ablation of brown adipocytes. In accordance with previous data (**Fig. 4e**), surface temperature was higher in P-CE vs. Ctrl offspring after CL injection (**Fig. 4g**), and the effect was lost when brown adipocytes were ablated (**Fig. 4h**). Lastly, we could show that DTA injection did not induce overt inflammation in mice (**Supplementary Fig. 4g**). Taken together, our data demonstrate that the effect of P-CE on respiration and thermogenesis is at least in part mediated through the activation of brown adipocytes.

P-CE protects from diet-induced obesity and insulin resistance

As BAT has been implicated in energy expenditure, we aimed to assess whether body weight and metabolism would be different under challenged conditions. Therefore, we fed P-CE and Ctrl offspring a high-fat diet (HFD), with 60% of the calories derived from fat, for 10 weeks. Even though P-CE offspring consumed significantly more food than Ctrl offspring (**Fig. 5a**), we found that P-CE-derived offspring exhibited a slightly lower body weight gain and reduced fat mass compared to Ctrl (**Fig. 5b**,**c**). Furthermore, we could show that P-CE offspring had markedly better insulin sensitivity (**Fig. 5d**), even though fasting blood glucose levels were unchanged. The latter might be due to the lower levels of circulating insulin in P-CE offspring (**Fig. 5e**). We found significantly lower levels of circulating TAGs in P-CE vs. Ctrl offspring (**Fig. 5f**), while cholesterol levels remained unchanged (**Fig. 5g**).

Intriguingly, we observed a significantly higher metabolic rate indicated by higher VO_2 and VCO_2 levels at RT conditions in P-CE vs Ctrl offspring (**Fig. 5h** and **Supplementary Fig. 5a**), while we did not observe any changes in substrate utilization, as indicated by an unchanged RER (**Supplementary Fig. 5b**). This higher oxygen consumption rate (OCR) was paralleled by significantly higher body surface temperature (**Supplementary Fig. 5c**) and UCP1 expression in iBAT (**Supplementary Fig. 5d**). Furthermore, we could show that hepatic lipid accumulation was reduced in P-CE vs. Ctrl offspring (**Fig. 5i**,**j**), which might explain the altered insulin sensitivity. Notably, circulating levels of FGF21, a hormone which has been suggested to be secreted from activated BAT[26] and is known to affect glucose and lipid homeostasis, was higher in P-CE offspring kept on a high fat diet (**Fig. 5k**). Taken together, our data demonstrate that

under RT conditions, which give mild cold stress, P-CE offspring are partially protected from diet induced obesity and maintain an improved metabolic profile.

Gene expression and DNA methylation analysis of P-CE offspring suggests changes in brown adipocyte formation and neurogenesis

Based on our data, we asked whether transcriptional changes in iBAT could explain the observed phenotype. Therefore, we performed RNA sequencing (RNA-seq) of iBAT from P-CE and Ctrl offspring at RT and after a 3-day CE. Unbiased hierarchical clustering including all genes expressed in at least one sample group revealed distinct transcriptional profile of the different conditions (**Supplementary Fig. 6a**). A principal component (PC) analysis similarly showed distinct clusters of each of the 4 sample groups (**Fig. 6a**). PC1 appeared to capture differences imposed by acute cold exposure. Several genes related to BAT activity, such as glycerol kinase (*Gyk*) or *Ucp1* were major contributors of negative PC1 loadings, while muscle specific genes contributed to positive PC1 loadings. Interestingly, samples from P-CE offspring after CE had an even stronger negative PC1 loading than the Ctrl samples, indicating a hyperactivated BAT condition in P-CE offspring.

A pairwise differential gene expression analysis comparing Ctrl-RT vs. Ctrl-CE, considering significant hits with at least a 2-fold mean expression difference (**Supplementary Table 1**), identified many genes related to BAT activity (**Supplementary Fig. 6b**,**c**). In line with the PC analysis, we also found a number of genes upregulated in the CE samples from P-CE offspring compared to Ctrl offspring related to BAT activity (**Fig. 6b**) and an enrichment of gene ontology (GO) terms related to high metabolic activity in all significantly regulated genes (**Fig. 6c**). Of note, *Adrb3*

283 and *Ucp1* were also significantly differentially expressed, however the regulation was
284 <2-fold between P-CE-CE and Ctrl-CE, therefore these genes were not included in the
285 GO analysis.

286 As phenotypic and transcriptional changes of P-CE in the offspring are mediated
287 through the sperm via the paternal lineage, we performed whole-genome bisulphite
288 sequencing of sperm (6-fold average genomic coverage in each sample) to identify
289 possible DNA methylation alterations which could potentially mediate the
290 intergenerational transmission of the observed phenotype (**Fig. 6d**). We observed a
291 small but significantly greater degree of global 5'-cytosine-phosphate-guanine-3' (CpG)
292 DNA methylation in the P-CE samples (89.5% vs 87.5%; *P*-value < 0.002; **Fig. 6e**),
293 indicating an effect of cold exposure on the sperm methylome.

294 To analyze whether methylation levels were altered in genomic regions which
295 might affect gene expression in the offspring, we first performed hierarchical clustering
296 and PC analysis of the methylation status of all promoter regions (**Fig. 6f** and
297 **Supplementary Fig. 6d**). We observed a clear separation between P-CE and Ctrl
298 sperm samples and a distinguishable clustering of the two groups in the PC analysis. In
299 contrast to global CpG methylation, we found a small, but significant reduction in the
300 average methylation levels of CpG islands (CGI) in P-CE samples (**Supplementary Fig.**
301 **6e**). Hierarchical clustering and PC analysis of all non-CGI promoters showed
302 comparable levels of separation on PC1 but less clear clustering, suggesting that the
303 differences in CGI methylation are relevant contributors to the observed differences in
304 promoter methylation.

305 These analyses indicate that the cold exposure induced methylation changes in
306 sperm are reproducible and contribute to the observed phenotypic differences in the

offspring. It is important to note that sperm is a haploid cell type and as such, single CpG sites can only be either methylated or unmethylated. To address this issue, we decided to subdivide the genome in probes of 50 adjacent CpGs and analyze methylation changes over these probes. An unbiased analysis of the P-CE and Ctrl sperm methylome datasets identified 2431 DMRs with an overlapping or downstream (max. 2kbp) gene (**Fig. 6g** and **Supplementary Table 2**). GO enrichment analysis of DMRs hypomethylated in P-CE samples related to many "neurogenesis" terms (**Fig. 6g**). A specific analysis of *Adrb3*, an important regulator of BAT activity, revealed local hypomethylation in the coding region (False discovery rate (FDR) = 0.01). An independent pyrosequencing analysis of individual CpG sites at the *Adrb3* locus in sperm samples confirmed this result (**Supplementary Fig. 6f)** and showed that the CpGs at the *Adrb3* locus were hypomethylated in adult iBAT and ingWAT from P-CE animals (**Supplementary Fig. 6g**,**h)**. Interestingly, the transcriptomic analysis had shown that *Adrb3* was also significantly higher expressed in P-CE iBAT (**Fig. 2c** and **Fig. 6b**). To test whether this effect was mediated by DNA methylation, we generated an *Adrb3* overexpression plasmid with a CpG-free backbone and in vitro methylated all CpGs. We then transfected the methylated and non-methylated plasmids into cells not expressing *Adrb3* (**Supplementary Fig. 6i**) and confirmed the methylation status of the CpG sites in the transfected plasmids (**Supplementary Fig. 6j**). We found that expression of *Adrb3* from the methylated plasmid was significantly lower than from the unmethylated plasmid, suggesting that DNA methylation at the *Adrb3* locus influences *Adrb3* expression.

Next, we elucidated whether the differential methylation status in the sperm of P-CE and Ctrl samples was directly correlated with transcriptional changes in iBAT tissue.

Therefore, we analyzed the expression levels of genes overlapping with DMRs either hypermethylated or hypomethylated in P-CE sperm. Interestingly we found that the average expression levels of transcripts overlapping with hypermethylated sperm P-CE DMRs were significantly increased compared to all transcripts, while inversely, transcripts overlapping with hypomethylated DMRs were significantly lower expressed in iBAT tissue (**Fig. 6h**). Gene body methylation is a feature of transcribed genes, even though the exact functions are not known[27,28], and it is therefore possible that the identified sperm DMRs could contribute to the greater formation of iBAT tissue in P-CE animals, and might contribute to the observed intergenerational effect. We also found a number of transcripts being significantly differentially expressed (DE) in the iBAT of P-CE vs Ctrl CE samples and overlapping with hypo- or hypermethylated DMRs in the respective sperm samples, highlighting a potential direct effect of germline methylation levels and iBAT expression levels for selected genes (**Fig. 6i**). Taken together, our analyses support our findings that iBAT from P-CE mice is hyper-activated and in part dependent on enhanced brown adipocyte formation, reflected by the upregulated brown markers and downregulated muscle specific genes, possibly due to increased neuronal innervation.

P-CE leads to a cell autonomous increase in brown adipocyte formation

To assess whether brown adipocyte formation is indeed altered in P-CE offspring, we isolated stromal vascular fraction (SVF) from iBAT of P-CE and Ctrl mice and differentiated these cells into mature brown adipocytes, *ex vivo*. When we analyzed lipid droplet staining, we did not observe any differences in either cell numbers or the appearance of multilocular cells (**Supplementary Fig. 7a-c**). However, we observed a

significant increase in the percentage of UCP1-positive cells, but not the average intensity of UCP1 staining in UCP1$^+$ cells (**Supplementary Fig. 7a**,**d**,**e**), suggesting an increased propensity to form brown adipocytes. We observed a significant induction of UCP1 protein and mRNA in P-CE offspring derived cells (**Supplementary Fig. 7f**,**g**). Similar to UCP1 we observed a higher *Adrb3* and cell death-inducing DFFA-like effector a (*Cidea*) mRNA expression, while peroxisome proliferator-activated receptor γ (*Pparγ*) levels were the same (**Supplementary Fig. 7h**-**j**).

To analyze whether these changes would translate into altered functionality, we quantified the OCR of these *ex vivo* differentiated cells. While we did not observe any changes in basal OCR, we could show that cells from P-CE offspring had a significantly higher OCR under CL stimulated conditions (**Supplementary Fig. 7k**).

To confirm these findings, we quantified ADRB3 protein levels in P-CE and Ctrl offspring. In accordance with the mRNA data, we observed a higher ADRB3 protein expression in P-CE vs. Ctrl offspring at RT, CE and TN conditions (**Supplementary Fig. 7l**). Given the widespread expression of *Adrb3* we also analyzed expression in ingWAT, epididymal adipose tissue (epiWAT) and heart (**Supplementary Fig. 7m**) and could show an up-regulation of *Adrb3* mRNA expression in ingWAT and epiWAT, but not in heart. To analyze whether this regulation could be connected to the DMR pattern which suggested an alteration in neurogenesis related genes, we analyzed tyrosine hydroxylase (TH) expression in iBAT from P-CE vs. Ctrl offspring, which was increased at both RT and after 2 days CE (**Supplementary Fig. 8a**) and we observed higher TH-immunostaining in neuronal axons within iBAT (**Supplementary Fig. 8b**,**c**). We checked vascularization by staining with isolectin B4 (IB4) and could show that iBAT from P-CE offspring was enriched with blood vessels (**Supplementary Fig. 8d**,**e**). These data

suggest that iBAT from P-CE offspring is more densely innervated and vascularized, which could explain the hyper-active state.

To test this hypothesis at a functional level, we performed microdialysis of iBAT from P-CE and Ctrl offspring. We observed an increased release of norepinephrine in P-CE offspring in response to a cold stimulus (**Supplementary Fig. 8f**). Furthermore, when we blocked adrenergic signaling *in vivo*, either with a selective ADRB3-antagonist L748,337 or an unspecific beta-blocker propranolol prior to CE, we observed that similar to BAT ablation, pretreatment with L748,337 or propranolol blocked the effect of P-CE on OCR (**Supplementary Fig. 8g**,**h**). Taken together, these data demonstrate that P-CE leads to higher neuronal innervation and norepinephrine release in iBAT of P-CE-derived offspring, while blocking beta-adrenergic receptor signaling in general, or ADRB3 in particular, abrogates the effect of P-CE.

Discussion

Paternal adaptation to environmental cues have been linked to various physiological changes in the offspring utilizing different animal model systems[22,29]. Our data indicate that CE can be a determinant of the offspring's physiology. This finding is in line with a recent study suggesting that seasonality can affect systemic metabolism[23,30-33] and that temperature sensing might influence physiological adaptation. A possible implication for clinical weight-loss studies could be randomization stratified by birth season, however such a mechanism would have to be investigated in a prospective trial. Furthermore, despite the large number of individuals studied in our cohort and the low *P*-value, our results still need to be interpreted with caution. First, the retrospective nature of the study and the inclusion of individuals undergoing FDG-PET/CT introduces numerous

biases. Since BAT was not specifically stimulated, an unknown proportion of "BAT-negative" labelled individuals may still have functional but inactive BAT. Second, the location of birth and conception are unknown, which is problematic as there were at least two major immigration waves to Switzerland from southern parts of Europe in the past century[34]. Third, the climate in Switzerland varies significantly ranging from a mild, Mediterranean-like climate to arctic conditions. Moreover, the clothing style of individuals may not always correlate with the absolute outside temperature, but rather with the perceived meteorological season. Lastly, the amount of daylight has been shown to negatively correlate with BAT activation[35] and is an inseparable confounder in this kind of retrospective cohort study.

Based on our data we propose that pre-conception CE of male mice leads to a higher degree of inducibility of brown fat which is in line with previous work demonstrating that seminal plasma can be the carrier for phenotypic alterations[36]. A possible explanation for the lack of transmission via the maternal lineage is the anatomical location of testis, which is directly exposed to changes in temperature[37]. Nevertheless, it remains unclear whether sperm directly senses temperature or whether the effect is due to a signal derived from other cells. While *de novo* methylation is initiated around E13.5 in mitotically arrested prospermatogonia and the methylome is completely established prior to birth, *de novo* methylation is not initiated until after birth in the female germline. As a result, the sperm methylome is dependent on faithful DNA methylation maintenance while the oocyte methylome is purely reflective of *de novo* methylation events. Furthermore, it should be noted that CE does generally not have the capacity to promote genetic mutations; therefore, the observed phenomenon is not driven by genetic inheritance but by (environmental) epigenetic inheritance.

427 The observed relative increase in basal brown fat UCP1 protein expression at RT
428 in P-CE offspring might be due to the fact that 23°C constitutes a mild cold challenge to
429 mice[38]. The observed reduction in circulating triacylglycerols (TAGs) is in line with a
430 previous report demonstrating that BAT is a major sink for TAGs[39], while the higher
431 NEFA levels during fasting in P-CE vs Ctrl mice could be due to enhanced Adrb3
432 signaling in white adipose tissue.

433 Multiple studies have implicated that BAT plays an important role in metabolism,
434 however, very few studies have quantified the actual contribution of BAT. Since *Ucp1*
435 deletion requires breeding and housing at TN, use of *Ucp1*-ko mice might influence the
436 physiological response[40]. By using an acute model of DTA targeted ablation exclusive to
437 brown and active brite adipocytes[25], we were able to show that BAT at least in part
438 mediates the observed metabolic changes, even though changes in heart, white fat or in
439 inflammatory responses could account for parts of the metabolic alterations.

440 Based on our results, we propose that paternal cold induces a hyperactive state
441 in brown adipose tissue of the offspring, which leads to improved adaptation to
442 overnutrition and hypothermia. Various DMRs did overlap with or are in close proximity
443 to genes annotated for neurogenesis. Furthermore, the observed denser neuronal
444 innervation, higher vascularization and increased norepinephrine release in iBAT[41],
445 highlight that multiple genes contribute to this complex phenotype. Together these
446 results suggest the CE affects the sperm methylome, raising the possibility that altered
447 sperm DNA methylation in CE fathers contributes to the observed phenotype. It is worth
448 noting that this is, to our knowledge, the first example in which adult CE leads to
449 significant alterations in sperm methylation. While recent studies have shown that
450 "epivariation", i.e. stochastic individual differences in DNA methylation, can be the major

contributor to the sperm methylome[42], we would like to point out that the significant concordant global methylation changes, as well as the clear separation of promoter methylation profiles in sperm of P-CE mice vs. Ctrl animals, suggest a direct effect of CE on the sperm methylome. Nonetheless, whether these modifications are causative or whether other epigenetic modifications, which can convey inherited traits[43], such as histone modifications[44] or long non-coding and small RNAs[45] contribute to the observed phenotype, remains to be analyzed.

The phenomenon identified here may also have implications for evolutionary biology as adaptation to environmental temperature changes is critical for any organism. Intergenerational memory of past CEs, may have been one mechanism to improve the survival of the offspring, during prolonged phases of cold exposure, such as the ice age 2.6 million years ago. In conclusion, through modulation of genetic and epigenetic variances, environmental changes might influence adipose tissue and metabolism not only in the exposed individual but also in the next generation. Such mechanisms might be exploitable to design therapies and personalized strategies to induce BAT functionality to counteract obesity and co-morbidity diseases.

Acknowledgements

We are grateful to M. Stoffel, J. Krützfeldt and members of the Wolfrum lab for helpful discussion. We would also like to thank K. Tabbada for assistance with WGBS high-throughput sequencing and F. Krueger and S. Andrews for help with bioinformatics analysis. We thank K. De Bock and F. Zheng for IB4 antibody. We thank K.A. Rollins for editing the manuscript. Data produced and analyzed in this paper were generated in collaboration with the Genetic Diversity Centre (GDC) and Functional Genomics Center

Zurich (FGCZ). The work was supported by the Swiss National Science Foundation (SNSF, CW and FvM).

Author Contributions

W.S. and C.W. designed the study. W.S. and H.D. performed all experimental work except the following. P.P. performed IVF. S.M. helped with the seahorse experiments. D.H.D. performed the Ucp1-DTR-GFP mice characterization. C.W., V.E., M.B., and D.H.D. contributed to radio labeled glucose tracing. E.K. did paraffin sectioning. G.G. did lipid droplet size quantification. A.P. helped with FACS. V.E. performed automated image analysis. L.G.S. helped with indirect calorimetry analysis. G.S. helped in the analysis of maternal behavior. D.P.-R. and W.S. did the microdialysis studies. A.S.B., I.A.B., S.B. and C.Z. carried out the retrospective analysis of BAT in humans. W.S and C.W wrote the manuscript. L.O. contributed to RNA-seq data analysis. F.v.M. and W.R. did DNA methylation sequencing and bioinformatic analysis. F.v.M, A.S.B., I.A.B., D.H.D., S.M., M.B. and L.B. helped with manuscript editing.

Conflict of Financial Interests statement

The authors have NO affiliations with or involvement in any organization or entity with any financial interest or non-financial interest in the subject matter or materials discussed in this manuscript.

References

1. WHO. Obesity and overweight Fact sheet. (2018).

2. Rosen, E.D. & Spiegelman, B.M. What we talk about when we talk about fat. *Cell* **156**, 20-44 (2014).

3. Tseng, Y.H., Cypess, A.M. & Kahn, C.R. Cellular bioenergetics as a target for obesity therapy. *Nat Rev Drug Discov* **9**, 465-482 (2010).

4. Frontini, A. & Cinti, S. Distribution and development of brown adipocytes in the murine and human adipose organ. *Cell Metab* **11**, 253-256 (2010).

5. Bartelt, A. & Heeren, J. Adipose tissue browning and metabolic health. *Nat Rev Endocrinol* **10**, 24-36 (2014).

6. Cannon, B. & Nedergaard, J. Brown adipose tissue: function and physiological significance. *Physiological reviews* **84**, 277-359 (2004).

7. Rosenwald M, W.C. The origin and definition of brite versus white and classical brown adipocytes. . *Adipocyte* **30**, 1 (2013).

8. Hany, T.F.*, et al.* Brown adipose tissue: a factor to consider in symmetrical tracer uptake in the neck and upper chest region. *European journal of nuclear medicine and molecular imaging* **29**, 1393-1398 (2002).

9. Cypess, A.M.*, et al.* Identification and importance of brown adipose tissue in adult humans. *N Engl J Med* **360**, 1509-1517 (2009).

10. Saito, M.*, et al.* High incidence of metabolically active brown adipose tissue in healthy adult humans: effects of cold exposure and adiposity. *Diabetes* **58**, 1526-1531 (2009).

11. van Marken Lichtenbelt, W.D.*, et al.* Cold-activated brown adipose tissue in healthy men. *N Engl J Med* **360**, 1500-1508 (2009).

12. Virtanen, K.A.*, et al.* Functional brown adipose tissue in healthy adults. *The New England journal of medicine* **360**, 1518-1525 (2009).

13. Zingaretti, M.C.*, et al.* The presence of UCP1 demonstrates that metabolically active adipose tissue in the neck of adult humans truly represents brown adipose tissue. *FASEB J* (2009).

14. Nedergaard, J., Bengtsson, T. & Cannon, B. Unexpected evidence for active brown adipose tissue in adult humans. *Am J Physiol Endocrinol Metab* **293**, E444-452 (2007).

15. Cypess, A.M.*, et al.* Activation of human brown adipose tissue by a beta3-adrenergic receptor agonist. *Cell Metab* **21**, 33-38 (2015).

16. Yoneshiro, T.*, et al.* Recruited brown adipose tissue as an antiobesity agent in humans. *J Clin Invest* **123**, 3404-3408 (2013).

17. Carone, B.R.*, et al.* Paternally induced transgenerational environmental reprogramming of metabolic gene expression in mammals. *Cell* **143**, 1084-1096 (2010).

18. Ng, S.F., *et al.* Chronic high-fat diet in fathers programs beta-cell dysfunction in female rat offspring. *Nature* **467**, 963-966 (2010).

19. Jaenisch, R. & Bird, A. Epigenetic regulation of gene expression: how the genome integrates intrinsic and environmental signals. *Nat Genet* **33 Suppl**, 245-254 (2003).

20. Seong, K.H., Li, D., Shimizu, H., Nakamura, R. & Ishii, S. Inheritance of stress-induced, ATF-2-dependent epigenetic change. *Cell* **145**, 1049-1061 (2011).

21. Anderson, L.M., *et al.* Preconceptional fasting of fathers alters serum glucose in offspring of mice. *Nutrition* **22**, 327-331 (2006).

22. Ng, S.F., *et al.* Paternal high-fat diet consumption induces common changes in the transcriptomes of retroperitoneal adipose and pancreatic islet tissues in female rat offspring. *FASEB J* **28**, 1830-1841 (2014).

23. Phillips, D.I. & Young, J.B. Birth weight, climate at birth and the risk of obesity in adult life. *Int J Obes Relat Metab Disord* **24**, 281-287 (2000).

24. Kaufman, M.H. <<*The*>> *atlas of mouse development*, (Academic Press, London <etc.>, 1994).

25. Rosenwald, M., Perdikari, A., Rulicke, T. & Wolfrum, C. Bi-directional interconversion of brite and white adipocytes. *Nat Cell Biol* **15**, 659-667 (2013).

26. Hondares, E., *et al.* Thermogenic activation induces FGF21 expression and release in brown adipose tissue. *J Biol Chem* **286**, 12983-12990 (2011).

27. Jones, P.A. Functions of DNA methylation: islands, start sites, gene bodies and beyond. *Nature reviews. Genetics* **13**, 484-492 (2012).

28. Yang, X., *et al.* Gene body methylation can alter gene expression and is a therapeutic target in cancer. *Cancer Cell* **26**, 577-590 (2014).

29. Ost, A., *et al.* Paternal diet defines offspring chromatin state and intergenerational obesity. *Cell* **159**, 1352-1364 (2014).

30. Lv, J., *et al.* The associations of month of birth with body mass index, waist circumference, and leg length: findings from the China Kadoorie Biobank of 0.5 million adults. *J Epidemiol* **25**, 221-230 (2015).

31. Speakman, J.R. & Heidari-Bakavoli, S. Type 2 diabetes, but not obesity, prevalence is positively associated with ambient temperature. *Sci Rep* **6**, 30409 (2016).

32. Valdes, S., *et al.* Ambient temperature and prevalence of obesity in the Spanish population: The Di@bet.es study. *Obesity (Silver Spring)* **22**, 2328-2332 (2014).

33. Yang, H.K., *et al.* Ambient Temperature and Prevalence of Obesity: A Nationwide Population-Based Study in Korea. *PLoS One* **10**, e0141724 (2015).

34. Afonso, A. *Immigration and its impacts in Switzerland*, (Duke Univ. Press, Washington DC, 2004).

35. Au-Yong, I.T.H., Thorn, N., Ganatra, R., Perkins, A.C. & Symonds, M.E. Brown Adipose Tissue and Seasonal Variation in Humans. *Diabetes* **58**, 2583-2587 (2009).

36. Adefuye, A.O., Sales, K.J. & Katz, A.A. Seminal plasma induces the expression of IL-1alpha in normal and neoplastic cervical cells via EP2/EGFR/PI3K/AKT pathway. *J Mol Signal* **9**, 8 (2014).

37. Zhang, Z.*, et al.* Functional analysis of the cooled rat testis. *J Androl* **25**, 57-68 (2004).

38. Fischer, A.W., Cannon, B. & Nedergaard, J. Optimal housing temperatures for mice to mimic the thermal environment of humans: An experimental study. *Mol Metab* (2017).

39. Bartelt, A.*, et al.* Brown adipose tissue activity controls triglyceride clearance. *Nat Med* **17**, 200-205 (2011).

40. Shabalina, I.G.*, et al.* UCP1 in brite/beige adipose tissue mitochondria is functionally thermogenic. *Cell Rep* **5**, 1196-1203 (2013).

41. Bronnikov, G., Houstek, J. & Nedergaard, J. Beta-adrenergic, cAMP-mediated stimulation of proliferation of brown fat cells in primary culture. Mediation via beta 1 but not via beta 3 adrenoceptors. *J Biol Chem* **267**, 2006-2013 (1992).

42. Shea, J.M.*, et al.* Genetic and Epigenetic Variation, but Not Diet, Shape the Sperm Methylome. *Dev Cell* **35**, 750-758 (2015).

43. Rando, O.J. Intergenerational Transfer of Epigenetic Information in Sperm. *Cold Spring Harb Perspect Med* **6**(2016).

44. Greer, E.L. & Shi, Y. Histone methylation: a dynamic mark in health, disease and inheritance. *Nature reviews. Genetics* **13**, 343-357 (2012).

45. Daxinger, L. & Whitelaw, E. Understanding transgenerational epigenetic inheritance via the gametes in mammals. *Nature reviews. Genetics* **13**, 153-162 (2012).

Figure 1

Parental cold exposure induces UCP1 expression in iBAT and ingWAT.

(**a**) The birthday frequency of individuals with no active BAT (no BAT) and active BAT (top panel) and the ratio of such individuals as a function of birth date (middle panel). BAT activity is measured by FDG-PET/CT (*n* = 8440 individuals, *P* = 1E-16). Monthly mean temperatures in Switzerland (bottom panel), to serve as a visual illustration of the warmer and colder periods. (**b**) BMI of BAT-negative (black boxes) and BAT-positive (green boxes) individuals born between April-September and October-March. Vertical bars are estimated 95%-CI's, The middle line represents the median, the top and bottom line the 75th and 25th percentile, respectively, the whiskers have the length 1.5 x interquartile range, *n* = 914 individuals, *P* = 0.00091, two-sided *t*-test, Bonferroni-corrected. (**c**) Scheme for the parental cold exposure mouse model. 10-week male and female C57BL/6 mice were cold stimulated for 0 (Group 1), 7 (Group 2), 14 (Group 3) and 21 days (Group 4) at 8 °C, then returned to 23 °C. Each block denotes 1 week; breeding was initiated at the end of the block 1. (**d**,**e**) Cropped western blots of UCP1 (γ-tubulin is the loading control) in the 4 experimental groups of offspring described in **c** from iBAT and ingWAT isolated while the mice were at RT (**d**) or after CE (**e**). Shown is one representative blot from four independent experiments, graphs depict mean of litter from all experiments ± standard error of mean (SEM), *n* = number of litters tested, each dot represents one litter. Statistical significance was calculated using one-way analysis of variance (ANOVA) test, (**d**-left) *n* = 7, $F_{(3,24)}$=6.48; (**d**-right) *n* = 8, $F_{(3,28)}$=3.52; (**e**-left) *n* = 8, $F_{(3,28)}$=10.90; (**e**-right) *n* = 8, $F_{(3,28)}$=8.65; Results are reported as mean ± SEM, * *P* < 0.05, ** *P* < 0.01, ***P* < 0.001.

Figure 2

Paternal cold exposure exclusively induces UCP1 expression in iBAT and ingWAT

(**a**,**b**) Either female (M-CE) or male (P-CE) mice were cold stimulated for 7 days before initiating a mating. All mice were kept at 23 °C afterwards. (**a,b**) Cropped western blots of UCP1 (γ-tubulin and HSP90 are the loading controls) in the 3 experimental groups of offspring of Ctrl, M-CE, and P-CE from iBAT and ingWAT isolated while the mice were at RT (**a**) or after CE (**b**). (**c**) mRNA levels of different brown fat markers in iBAT of Ctrl and P-CE offspring at RT, n = 8 litters, normalized by ΔCt values. (**d**) Cropped western blots of UCP1 (HSP90 is the loading control) in the *IVF* offspring of Ctrl and P-CE from iBAT at RT and after 2 days CE, (n = 11 litters for Ctrl and 10 litters for P-CE). (**e**-**h**) Representative H&E and UCP1 immunohistochemistry staining of (**e**,**g**) iBAT and (**f**,**h**) ingWAT, of Ctrl or P-CE offspring at (**e**,**f**) 23 °C and (**g**,**h**) 8 °C, scale bar 100 µm, n = litters per group. (**a**-left) n = 8, $F_{(2,21)}$ = 4.93, P = 0.018; (**a**-right) n = 8, $F_{(2,21)}$ = 3.92, P = 0.036; (**b**-left) n = 7, $F_{(2,18)}$ = 8.27, P = 0.003; (**b**-right) n = 8, $F_{(2,21)}$ = 7.74, P = 0.003; (**d**-left) P = 0.003; (**d**-right) P = 0.02. Throughout, data are mean ± SEM, each dot represents one litter, * P < 0.05, ** P < 0.01, and ***P < 0.001 by one-way analysis of variance (ANOVA) (**a**,**b**) or by two-tailed unpaired Student's t-test (**c**,**d**).

Figure 3

Paternal cold exposure induces oxygen consumption in offspring upon cold or ADRB3-agonist stimulation

(**a**) Representative thermographic image of Ctrl and P-CE offspring at postnatal day 7. Offspring were kept at RT, right inset depicts calculated averages of surface temperature, n = 7 litters, P = 0.04. (**b**) Representative thermographic image of Ctrl and

P-CE offspring at 23 °C and after 30h of CE, *n* = 7 litters, *P* (30h CE) = 0.03. (**c**) Time resolved oxygen consumption in Ctrl and P-CE offspring mice, with cold induction (arrow) followed by warm adaption (arrow), *P* = 0.006, dark phase is marked as dark background, right inset depicts calculated means as indicated, *n* = 5 litters. (**d**) Cropped western blots of UCP1 (HSP90 is the loading control) of iBAT from Ctrl and P-CE offspring, injected with saline or CL (0.1 mg/kg body weight, 3 times, every 24 h, *n* = 7 litters). (**e**) Time resolved Oxygen consumption of Ctrl (*n* = 4 litters) and P-CE (*n* = 5 litters) offspring, with CL (arrow), *P* = 0.003. (**f**) Representative UCP1 staining of iBAT of Ctrl or P-CE offspring with CL injection, scale bar 100 µm, *n* = 6 litters per group. (**g**) Serum NEFAs level of fasted (12h) and refeeding (4h) animals from Ctrl (*n* = 7 litters) and P-CE (*n* = 8 litters). (**h**) Glucose uptake in BAT at RT, 1 day and 3 days of CE (*n* = 7 litters for all groups, except *n* = 8 for P-CE at RT and 1 day CE). (**i**) Western blots of GLUT4 (HSP90 is the loading control) of iBAT isolated from Ctrl or P-CE offspring at RT and after 3 days of CE, *n* = 4 litters. Results are reported as mean ± SEM, each dot represents one litter. Statistical significance was calculated using a two-tailed unpaired Student's *t*-test; * $P < 0.05$, ** $P < 0.01$.

Figure 4

Paternal cold exposure induces oxygen consumption in offspring due to increased BAT functionality

(**a**) Tissue wet weight (*n* = 4 mice, *P* = 0.000001) and (**b**) Cropped western blots of UCP1 (γ-tubulin is the loading control) of iBAT from Ucp1-DTR-GFP mice (11-weeks of age) with saline or diphtheria toxin A (DTA) injection. (**c**) Representative H&E and UCP1 staining of iBAT of Ucp1-DTR-GFP animal after saline or DTA injection, scale bar, 100

µm, *n* = 4 mice. (**d**) Time resolved oxygen consumption in Ucp1-DTR-GFP Ctrl (*n* = 4 litters) and P-CE (*n* = 5 litters) offspring with cold induction (TP I) followed by three DTA injections (TP II-IV), light cycle (L), dark cycle (D) right inset depicts calculated means as indicated, dark phase is marked as dark background, *P* = 0.04. (**e**) Time resolved oxygen consumption in Ucp1-DTR-GFP Ctrl and P-CE offspring with CL injection (TP I) followed by three DTA+CL injections (TP II-IV), right inset depicts calculated mean as indicated, *n* = 4 litters, *P* = 0.03. (**f**) Time resolved oxygen consumption in Ucp1-DTR-GFP Ctrl and P-CE offspring 24 hour after BAT depletion (TP IV, **e**) and stimulated with CL (arrow), *n* = 4 litters. (**g**, **h**) Representative thermographic image of Ctrl and P-CE offspring with CL stimulation (**g**) before and (**h**) after BAT depletion, lower insets depict calculated averages, *n* = 8 litters. Results are reported as mean ± SEM. Statistical significance was calculated using a two-tailed unpaired Student's *t*-test; * *P* < 0.05, ****P* < 0.001.

Figure 5

Paternal cold exposure protects offspring from high fat diet induced obesity

(**a**-**c**) Daily (**a**) food intake, (**b**) body weight gain and (**c**) body composition of Ctrl and P-CE offspring mice fed a high fat diet, at RT for the indicated time. (**a**) *n* = 12, (**b**) *n* = 11, (**c**) *n* = 6 (**d**) Insulin tolerance test of Ctrl or P-CE offspring fed a HFD for 7 weeks at RT, 6h fasting, *n* = 12. Shown is one representative from three independent experiments. (**e**-**g**) Circulating (**e**) Insulin, (**f**) TAG and (**g**) Cholesterol levels of Ctrl or P-CE offspring fed a HFD for 11 weeks at RT. (**e**) *n* = 12, (**f**) *n* = 11, (**g**) *n* = 9. (**h**) Time resolved oxygen consumption time course and analysis, of Ctrl or P-CE offspring fed a HFD for 11 weeks at RT, right inset depicts calculated mean as indicated, *n* = 5, *P* = 0.001. (**i**)

Representative Oil red O staining on liver sections, of Ctrl or P-CE offspring fed a HFD for 11 weeks at RT, scale bar 200 µm, *n* = 6 litters. (**j**) TAG content in liver, *n* = 6. (**k**) Circulating FGF21 levels of Ctrl or P-CE offspring on HFD, *n* = 9. Results are reported as mean ± SEM, *n* = number of litters tested, each dot represents one litter. Statistical significance was calculated using a two-tailed unpaired Student's *t*-test; * $P < 0.05$, ** $P < 0.01$, *** $P < 0.001$.

Figure 6

Paternal cold exposure affects the transcriptional signature of the brown adipose tissue in the offspring and the epigenetic profile of the sperm

(**a**) Principal component analysis (PCA) of RNA-seq data from brown adipose tissue (BAT) samples. PC1 and PC2 for each sample were calculated using the SeqMonk PCA analysis pipeline, *n* = 6 litters. (**b**) Scatter plot of RNA-seq data from BAT samples, comparing P-CE vs CTRL samples following 3 days of cold exposure (3CE). Plotted are the log2-transformed normalized reads per million (RPM). Significant differentially expressed genes (overlap between DEseq2 and EdgeR) with at least 2-fold mean expression differences are highlighted in red. Selected genes of interest which do not fulfill all of the above criteria are labeled in blue and or only shown for comparison with the literature, *n* = 6. (**c**) GO terms of up and down regulated genes in P-CE-CE against Ctrl-CE samples, *n* = 6 litters. (**d**) Heatmap showing the methylation levels in DMRs between P-CE and Ctrl sperm samples. Clustering of DMRs was performed in SeqMonk. (**e**) Box whisker plots showing the CpG methylation levels of individual replicates of sperm samples from P-CE and Ctrl samples. Methylation was quantitated over consecutive probes spanning 50 CpGs. Significance was calculated using the

mean CpG methylation levels of P-CE vs Ctrl samples using a two-tailed unpaired Students *t*-test, *n* = 6 mice, *P* = 0.00052. (**f**) Hierachical clustering of promoter CpG methylation levels. (**g**) GO terms of hyper and hypo DMRs in P-CE over RT sperm, *n* = 6 mice. (**h**) Expression levels of transcripts in BAT samples overlapping with sperm DMRs either hypermethylated or hypomethylated in the paternal cold exposure vs control samples. Shown are the log2 RPM gene expression levels in BAT. Significance was calculated from the average gene expression levels of each group using a two-tailed unpaired Students *t*-test. *n* = 6 mice, number of all expressed genes is 11334, number of genes overlapping P-CE Hypermethyalted Sperm DMRs is 1049, number of genes overlapping P-CE Hypomethyalted Sperm DMRs is 365, "All expressed genes" vs "Genes overlapping P-CE Hypermethyalted Sperm DMRs": *P* = 3.7E-14, "All expressed genes" vs "Genes overlapping P-CE Hypomethyalted Sperm DMRs": *P* = 1.4E-6. Any individual points that fall outside this range are shown as filled circles. Each circle represents a single probe. (**i**) Scatter plot of RNA-seq data from BAT samples, comparing P-CE vs CTRL samples following 3 days of cold exposure (3CE). Plotted are the log2-transformed normalized reads per million (RPM). Highlighted are all genes which are significant differentially expressed (overlap between DEseq2 and EdgeR with at least 2-fold mean expression differences) between P-CE-3CE and Ctrl-3CE samples and overlap with identified sperm DMRs. (**e**,**h**) box plots of the CpG methylation percentages of tiling probes spanning 50 CpGs each. The middle line indicates the median of the data, the upper and lower extremities of the box show the 25th and 75th percentiles, and the upper and lower black whiskers show the median ± the interquartile range (25%–75%) multiplied by 2. ***$P < 0.001$.

CONTACT FOR REAGENT AND RESOURCE SHARING

For further information and requests for reagents generated in this study, please contact lead contact Christian Wolfrum (christian-wolfrum@ethz.ch).

METHODS

Materials

Details of the reagents used in this study are listed in Life Sciences Reporting Summary.

Human study

13502 ^{18}FDG-PET/CT scans of 8440 individuals examined during Nov.-Feb. in the years 2007 – 2015 were reviewed for the presence of active BAT by physicians[46]. Uptake in the supraclavicular and cervical area was considered grade 1, paravertebral, mediastinal grade 2 and infradiaphragmal grade 3. Readers were blinded to the hypothesis of this study. The birthdates of the individuals were extracted from the DICOM (Digital Imaging and Communications in Medicine) metadata of the images. Density plots of the birthdays were created with ggplot2 2.1.0 in R 3.3.1. (R Foundation for Statistical Computing, Vienna, Austria). The distributions of individuals were examined with a generalized linear model (Poisson error distribution and link function) to estimate the likelihood of being conceived in the cold period of the year. The BAT negative control cohort was matched for sex and age with the nearest neighbor algorithm[47]. The mean temperature of northern Switzerland was acquired from the federal meteorological in a monthly resolution. The study was approved by the Cantonal Ethics Committee Zürich.

Mice

C57BL/6N wild-type mice were obtained from Charles River. Ucp1-DTR-GFP mice were generated as described previously[25]. Unless indicated otherwise, all experiments were performed with adult male mice kept on an inverted 12h dark/light cycle, fed *ad libitum*

chow diet or 60% high fat diet. For cold stimulation, animals were housed in long type II cages at 8°C. All animal studies were approved by the Veterinäramt Zürich.

Primary adipocyte culture/HEK 293 cell culture

For cellular separation, dissected adipose tissues were minced with a scalpel blade and incubated in 2.0 ml/mg (wet tissue) 0.2% collagenase type II in collagenase buffer (25 mM $KHCO_3$, 12 mM KH_2PO_4, 1.2 mM $MgSO_4$, 4.8 mM KCl, 120 NaCl, 1.2 mM CaCl2, 5 mM glucose, 2.5% BSA, 1% Pen/Strep, pH 7.4) for 50 min at 37°C with occasional resuspension. 10 ml centrifugation buffer (70% PBS, 15% FBS, 15% HistoPaque 1119) was added and samples were centrifuged 5 min at 200 g. The SVF pellet from the initial centrifugation was resuspended in 2 ml erythrocyte lysis buffer (154 mM NH_4Cl, 10 mM $KHCO_3$, 0.1 mM EDTA, pH 7.4) and incubated for 4 min on ice. Samples were filtered through 40 µm cell strainers and centrifuged for 5 min at 200 g. Supernatant was removed and the pallets were resuspended in culture media, SVF cells were plated in a plate pre coated with collagen I and differentiated as described previously[48]. Cells were re-fed every 48 hours with 1µM rosiglitazone and 0.5µg/ml insulin. Fully differentiated adipocytes were stimulated with CL-316,243 (10nM) at day 8 (iBAT).

Human HEK 293A cell line (Invitrogen) were grown at 37°C, 5% CO2 in DMEM supplemented with 10% FBS and 1% penicillin/streptomycin. All cells in culture were routinely screened for mycoplasma contamination.

***In vitro* fertilization**

Spermatozoa isolated from cold-treated and control males were used to fertilize oocytes isolated from superovulated C57BL/6 females. The 4 week old females were

superovulated by i.p. administration of 5 IU of equine chorionic gonadotropin (PMSG) and 5 IU of human chorionic gonadotropin (hCG). Males were sacrificed, the dense sperm was isolated from cauda epididymis and capacitated in 200ul of Fertiup medium (Cosmo Bio) for 45 minutes at 37°C, 5% CO_2. Following sperm capacitation, 2ul of sperm solution was added to the *IVF* drop consisting of 100 ul HTF medium (Cosmo Bio) overlaid with embryo tested mineral oil (Sigma). The oviducts were immediately dissected, and the oocyte clutches released into the IVF drop. The IVF reaction was carried out for 4 hours at 37°C, 5% CO_2. Following the IVF, oocytes were washed several times in M16 medium and the efficiency of fertilization was ascertained by the appearance of the pronuclei and the 2nd polar body. Fertilized oocytes were surgically transferred into pseudopregnant CD1 foster females previously mated with genetically vasectomized Prnm1GFP males[49].

Body composition measurement

Body composition was measured with the EchoMRI 130 (Body Composition Analyzer, Echo Medical Systems). Mice were fasted for 4 hours before measurement.

Indirect calorimetry

Indirect calorimetry measurements were performed with the Phenomaster (TSE Systems) according to the manufacturer's guidelines and protocols. Animals were single caged and acclimated to the metabolic cages for 48 hours before metabolic recording.

Surface temperature measurement

807 Surface temperature was recorded with an infrared camera (E60; FLIR; West Malling,
808 Kent, UK) and analyzed with FLIR-Tools-Software (FLIR; West Malling, Kent, UK)[50].
809
810 **Radio labeled glucose tracing**
811 Tissue radiolabeled glucose uptake was measured as described previously[51]. Animals
812 were fasted for 4h, then ^{14}C-2-deoxyglucose at 8 mM, 14.8 MBq/kg body weight was
813 injected by tail vein. 30 minutes after injection, blood samples were collected, and mice
814 were sacrificed by cervical dislocation. iBAT, epiWAT, ingWAT, liver, skeletal muscle,
815 heart and the brain were dissected, weighed and lysed in 10 volumes of 0.5 M NaOH.
816 Radioactivity was measured by liquid scintillation counting (100 µl of lysate in 3.9 ml of
817 Emulsifier-Safe, Perkin Elmer).
818
819 **Insulin tolerance test (ITT)**
820 Animals were fasted for 4h (Chow diet) and 6h (High fat diet). Blood was collected from
821 a small incision in the tip of the tail (time 0) and then 15, 30, 60 and 120 min after an i.p.
822 injection of insulin at 0.6 U/kg (chow) and 0.75 U/kg (HFD) body weight, (Actrapid Penfill,
823 Novo Nordisk). Blood glucose levels were measured with a blood glucometer (Accu-
824 Chek Aviva, Roche).
825
826 **Behavioral studies**
827 Maternal behavior quantification was carried out as previously reported[52]. 9-week old
828 virgin female mice were bred with 9-week-old RT or P-CE male mice. All pregnant
829 females were single caged, and behavior was recorded throughout the pregnancy and

nursing by cameras. Maternal nursing behavior was quantified from delivery to postnatal day 11, based on the video recordings.

Plasma biochemistry analysis

Mice were fasted for 6h before sacrifice. Blood samples were obtained from cardiac puncture, and plasma was collected after centrifugation for 15mins at 3000rpm at 4°C. Cholesterol and triglycerides were measured by enzymatic tests (Roche Diagnostics). Plasma FGF21 was analyzed using Mouse/Rat FGF-21 ELISA kit (BioVendor). Plasma insulin levels were measured by Mouse/Rat insulin kit (Meso Scale Discovery). Plasma samples for measuring fasting/refeeding NEFAs was obtained after 12-h fasting and 4-h refeeding, by a commercial NEFAs kit (WAKO).

DNA isolation from sperm and adipose tissue

DNA from sperm and adipose tissue were extracted with the QIAamp DNA Mini Kit (Qiagen). Sperm samples were isolated from cauda epididymis, resuspended in M2 medium (Sigma) for 45 min at 37°C. Supernatant containing sperm without tissue debris were collected, pelleted (10,000 g), washed with washing buffer (150 mM NaCl, 10 mM EDTA pH 8.0), and centrifuged for 10 min at 4000 rpm. The sperm pellet was resuspended in 300 µl lysis buffer (100 mM Tris·Cl pH 8.0, 10 mM EDTA, 500 mM NaCl, 1% SDS, 2% ß-mercaptoethanol).

DNA pyro-sequencing

500ng DNA (from sperm, adipose tissues or HEK cells) was bisulfite-converted with the EpiTect Bisulfite Kit (Qiagen) following the manufacturer's protocol. 20 ng of this

bisulfite-converted DNA was PCR-amplified with the PyroMark PCR Kit (Qiagen). PCR amplification and sequencing primers (reverse primers were biotinylated) were designed using the Pyromark Assay Design v2.0 software (Qiagen). Quality of PCR products were checked by gel electrophoresis. Pyrosequencing was applied on a PyroMark Q96 ID using PyroMark Reagents (Qiagen). DNA methylation frequency was quantified with the PyroMark software (Qiagen). Specific CpG sites are illustrated in **Supplementary Table 3**.

In vitro methylation assay

Coding sequence of mouse Adrb3 DNA was ordered from Genscript and cloned into pCpGfree-mcs vector (Invivogen). HEK293 cells with 80% confluency in 24-well plates were transfected 1000 ng/well of either methylated or unmethylated constructs with PEI (Polysciences), at 4:1 ratio to DNA. 24 h after transfection, medium was replaced. Transfected cells were harvested for analysis at 48 h post transfection.

Tissue harvest

Animals were euthanized singly in a carbon dioxide atmosphere. Popliteal lymph nodes were removed from inguinal depots for analyses of gene expression and cellular separations. Blood was collected by cardiac puncture, and serum was obtained by centrifuging coagulated blood at 10,000g for 5 min at 4°C.

Analysis of adipocyte differentiation

Differentiated adipocytes at day 8 were used for differentiation analysis. Briefly, cells in 96 well optical plate were fixed with 5% formaldehyde at 4 °C for 10 min, followed by 3

878 times washing with PBS. Cells were stained with LD540 (100 ng/µl) for lipid droplets[53]
879 and Hoechst No. 33342 (100 ng/µl). For UCP1 staining, lipids were depleted by 5%
880 acetic acid in ethanol for 10 min at -20 °C, washed with PBS twice at RT and blocked in
881 0.05% triton, 5% BSA, PBS. Cells were incubated with UCP1 antibody (1:500) overnight,
882 washed trice in PBS, incubated with 488 anti-rabbit (1:500) secondary antibody and
883 DAPI, followed by three washing steps. 29 images per well were taken with an
884 automated microscope imaging system (Operetta, Perkin Elmer). Images were analyzed
885 using the Operetta imaging software as described previously[54].
886
887 **Histology and image analysis**
888 Adipose tissues were excised, fixed in fresh 4% paraformaldehyde (Sigma) in PBS
889 (Gibco; pH 7.4) for 24 h at 4°C and then embedded with paraffin. 4-micron paraffin
890 sections were subjected to histological staining[55]. Heat induced antigen retrieval was
891 applied on rehydrated paraffin sections. After blocking with 5% BSA for 1 hour, primary
892 antibody (1:200 UCP1, Thermo) diluted in 5% BSA was applied to sections overnight at
893 4 °C. After washing with PBS, a secondary antibody (Signal Stain Boost IHC, Cell
894 Signaling) was applied and the sections were washed 3 times and were detected using
895 the DAB method (Cell Signaling). Standard hematoxylin and eosin staining was
896 performed on rehydrated fat paraffin sections. Slides were dehydrated and covered with
897 coverslip by resin-based mounting. Analysis of lipid droplet sizes was performed using
898 ImageJ. For each treatment 21-33 pictures were analyzed. Approximately 18000-58000
899 lipid droplet objects per mouse were used for the computation of lipid droplet size. Oil
900 red O staining was applied on liver cyro-sections, as previously described[56]. Liver
901 samples were excised, fixed with PFA, dehydrated with 30% sucrose and embedded in

OCT. 10 µm sections were cut and stained with fresh prepared ORO staining solution. All images were acquired by Axioscope A.1.

Fluorescence immunostaining of adipose cryosections

Brown adipose tissues from Ctrl and P-CE animals were excised and fixed in fresh 4% paraformaldehyde (Sigma-Aldrich) in PBS (Gibco) at pH 7.4 for 2 h at 4 °C, washed four times in PBS and cryopreserved for 30 h in 30% sucrose in PBS with stirring at 4 °C. The samples were flash-frozen on dry ice and stored at −80 °C. Brown adipose tissues were cut at −25 °C on an HM 500 O microtome (Microm) at 20 µm thickness, mounted on Superfrost plus slides (Medite) and thawed at 4 °C, blocked with 10% donkey serum in PBS for 1 h, followed by tyrosine hydroxylase antibody overnight incubation 1:200 in PBS. Sections were washed 3 times in PBS at RT, stained with Alexa 488 anti-rabbit secondary antibody and 300 nM DAPI for 1 h. Slides were embedded in ProLong® Diamond Antifade Mountant (Themo). Fluorescence micrographs were acquired on an SP5 confocal microscope (Leica). Background was adjusted using samples without primary antibody.

Extracellular respiration

Primary brown preadipocytes were counted and plated at a density of 20,000 cells per well of a seahorse plate and differentiated to confluence. At day 8 post-differentiation induction, mature brown adipocytes were loaded to XF_{24} Extracellular Flux Analyzer (Seahorse Bioscience), with one injection of CL-316,243 (10 nM).

RNA extraction, cDNA synthesis, quantitative RT-PCR

Total RNA was extracted from tissues or cells using Trizol reagent (Invitrogen) according to the manufacturer's instructions. Reverse transcription was performed to generate cDNA library by using the High Capacity cDNA Reverse transcription kit (Applied Biosystems), with 1 µg of RNA. Quantitative PCR was performed on a ViiA7 (Applied Biosystems) and relative mRNA concentrations normalized to the expression of *36B4 (Rplp0)* were calculated by the ΔΔCt method. Primer sequences are listed in **Supplementary Table 4**.

RNA-Sequencing, Mapping and Analysis

RNA from brown adipose tissue were quality checked by tape station (GE). All samples had a RIN value of greater than 8. The ribosomal RNA was depleted, and purified RNA was used for the preparation of libraries using the TruSeq RNA sample preparation kit (Illumina) and sequenced on a HiSeq 4000 HT. RNA-seq sequences were trimmed using Trim Galor (v0.4.4, http://www.bioinformatics.babraham.ac.uk/projects/trim_galore/) and mapped to the mouse GRCm38 genome assemblies using hisat2 (v2.1.0). Transcripts were defined using the Ensemble annotations over protein-coding mRNAs. Differential expression analysis of mapped RNA-seq data was performed using DESeq2[57] and EdgeR. Significantly different transcripts were called with significance below 0.05 after Benjamimi and Hochberg correction and minimum mean differential expression of 2-fold. Further analysis were performed using SeqMonk software (www.bioinformatics.babraham.ac.uk/projects/seqmonk/). Quantitation of RPM values was performed using the SeqMonk RNA-Seq pipeline quantitation on merged transcripts counting reads over exons correcting for DNA contamination and log2 transformed

assuming an opposing strand specific library transformed by percentile normalization using “Add” to the 75.0 percentile. Gene ontology (GO) analysis were performed using the g:profiler software (http://biit.cs.ut.ee/gprofiler/). Expressed genes were defined where at least 1 of all 4 groups (CTRL-3CE, CTRL-RT, P-CE-3CE, P-CE-RT) had a log2(RPM) value above zero. Transcriptional similarities between the different samples were computed on all expressed genes using hierarchical clustering (R hclust package) with Euclidian distances and by applying the Ward distance function and plotted as a dendrogram. PCA was performed using the R prcomp package with default parameters.

Whole-Genome Bisulfite Sequencing

Mapping and Analysis Genomic sperm DNA was isolated as described and used for whole-genome bisulfite (WGBS) libraries[58]. Briefly, WGBS libraries were prepared by sonicating 500ng genomic DNA using a Covaris Sonicator into 300-400bp long fragments, followed by end-repair, A-tailing and methylated adapter (Illumina) ligation using NEB-Next reagents. Libraries were bisulfite treated using EZ DNA Methylation-Direct Kit (Zymo), followed by library amplification with indexed primers using KAPA HiFi Uracil+ HotStart DNA Polymerase (Roche). All amplified libraries were purified using AMPure XP beads (Agencourt) and assessed for quality and quantity using High-Sensitivity DNA chips (Agilent Bioanalyzer). High-throughput sequencing of all libraries was carried out with a 125 bp paired-end protocol on a HiSeq 2000 instrument (Illumina). Raw sequence reads from WGBS libraries were trimmed to remove poor quality reads and adapter contamination, using Trim Galore (v0.4.4, http://www.bioinformatics.babraham.ac.uk/projects/trim_galore/). The remaining sequences were mapped using Bismark (v0.18.0)[59] with default parameters to the

mouse reference genome GRCm38 in paired-end mode. Reads were deduplicated and CpG methylation calls were extracted from the deduplicated mapping output using the Bismark methylation extractor (v0.18.0) in paired-end mode. CpG methylation calls were analyzed using R and SeqMonk software (www.bioinformatics.babraham.ac.uk/projects/seqmonk/). The genome was divided into consecutive probes overlapping 50 CpGs each and percentage methylation was calculated using the bisulfite feature methylation pipeline in SeqMonk. Global CpG methylation levels were illustrated using box whisker plots and promoter methylation similarities between the samples were assessed using hierarchical clustering (R hclust with Pearson distances and Ward distance function) and PCA (R prcomp package with default parameters). CpG island (CGI) methylation levels were calculated using the SeqMonk bisulfite feature methylation pipeline and averaged over all CpG islands for illustrations. DMRs were calculated using the SeqMonk binomial filter on probes (50 CpG probes or CGIs) with significance below 0.05 after multiple testing correction and a minimum difference of 10%. Gene ontology analysis were performed using the g:profiler software (http://biit.cs.ut.ee/gprofiler/) with genes which either overlapped with DMRs or where up to 2kb downstream of the DMR. DMRs were divided into hypermethylated or hypomethylated in the paternal cold exposure vs control samples. The expression levels in brown adipose tissue samples of transcripts overlapping with DMRs (logistic regression filter; see above) either hypermethylated or hypomethated in the P-CE vs Ctrl samples was computed using the log2 RPM gene expression levels in Ctrl brown adipose tissue samples.

Western Blot

Protein samples were isolated from adipose tissue with RIPA buffer (50 mM Tris-HCl pH (7.5), 150 mM NaCl, 1mM EDTA, 1% Triton X-100, 0.1% SDS, 10% glycerol) supplemented with protease inhibitor cocktail (Roche) and Halt Phosphatase Inhibitor (Thermo). Homogenized protein lysates were obtained by rotating at 4 °C for 30 min, followed by centrifugation at 14,000 rpm for 30 min. Protein amounts were quantified using the DC Protein Assay (Bio-Rad). For immunoblotting, protein samples were separated by SDS-PAGE on 12% polyacrylamide gels and transferred onto nitrocellulose membrane. Membranes were probed using the indicated antibodies and chemiluminescent signals was detected by a LAS 4000 mini Image Quant system (GE Healthcare). Band intensity was quantified using ImageJ. Uncropped full scan blots are shown in **Supplemental Fig. 9-11.**

In vivo microdialysis from iBAT

For measuring the release of norepinephrine from iBAT a microdialysis probe was implanted subcutaneously on the back of the animal one hour before the start of the experiment (CMA 20 custom made, 3mm membrane, cutoff 20,000 kDa, CMA, Sweden). The microdialysis probe was connected to a pump that flushes artificial cerebrospinal fluid (147 mM Na^+, 2.4 mM Ca^{2+}, 4 mM K^+, 155.6 mM Cl^-, pH 6.0) through the probe at a follow rate of 1.5 ul/min. The tube was connected to the animal via a movable arm to allow free movement. After stabilization, samples were collected at 30-min intervals through a refrigerated fraction sampler (MAB 85, Microbiotech AB, Sweden). After baseline samples at RT were collected, temperature was reduced to 8°C for a period of 3-hours.

HPLC norepinephrine assessment

Dialysate samples from BAT were immediately frozen and stored at −80 ˚C until injection onto the high-performance liquid chromatography (HPLC; Ultimate 3000, Thermo Scientific, US) system. Norepinephrine levels were detected and analyzed using an electrochemical detector (ECD-3000RS, Thermo Scientific, US) with a coulometric cell (6011RS, Thermo Scientific, US). The samples were injected via a refrigerated autoinjector (Thermo Fisher, CA, USA) equipped with a 100 µl injection loop. Samples were separated on a reversed-phase column (4.6×80mm, 3µmThermo Fisher, US). We used a HPLC pump (ISO-3100BM, Thermo Fisher, CA, USA) and a mobile phase of ammonium acetate, EDTA, 15% methanol, 5% acetonitrile adjusted to pH of 6.0, at a flow rate of 0.3 ml/L at 32°C. A chromatography workstation (Chromeleon, Thermo Fisher Scientific, Switzerland) was used for data acquisition and calculation.

Statistical analyses

For *in vivo* studies, age-matched male mice were used for all experiments. Sample sizes were determined on the basis of previous experiments using similar methodologies. P-CE and Ctrl fathers always were derived from same litters and were handled in the same manner. One to two offspring were used from each litter for all experiments. The number of litters analyzed for all experiments are indicated in the corresponding figure legends. If more than one mouse from one litter was used the mice were analyzed as technical replicates. In total more than 60 litters per group were analyzed for P-CE and Ctrl mice, respectively. Mice were randomly assigned to treatment groups. All animals were included for statistical analyses, and the investigators were not blinded. RNA and DNA methylation sequencing analyses were blinded to experimental conditions. Results are

reported as mean ± SEM. Two-tailed unpaired Student's *t*-test was applied on comparison. ANOVA was applied on comparisons which involve multiple groups. Statistical differences were indicated as * for $P < 0.05$, ** for $P<0.01$ and *** for $P<0.001$.

DATA AND SOFTWARE AVAILABILITY

The accession number for the WGBS next-generation-sequencing data reported in this study is GEO: GSE100231. RNA sequencing data was uploaded to European Nucleotide Archive (ENA) with accession number PRJEB15274.

References for methods

46. Becker, A.S., Nagel, H.W., Wolfrum, C. & Burger, I.A. Anatomical Grading for Metabolic Activity of Brown Adipose Tissue. *PLoS One* **11**, e0149458 (2016).

47. Ho, D.E., Imai, K., King, G. & Stuart, E.A. Matching as nonparametric preprocessing for reducing model dependence in parametric causal inference. *Polit Anal* **15**, 199-236 (2007).

48. Kazak, L.*, et al.* A creatine-driven substrate cycle enhances energy expenditure and thermogenesis in beige fat. *Cell* **163**, 643-655 (2015).

49. Haueter, S.*, et al.* Genetic vasectomy-overexpression of Prm1-EGFP fusion protein in elongating spermatids causes dominant male sterility in mice. *Genesis* **48**, 151-160 (2010).

50. Whittle, A.J.*, et al.* BMP8B increases brown adipose tissue thermogenesis through both central and peripheral actions. *Cell* **149**, 871-885 (2012).

51. Abreu-Vieira, G.*, et al.* Cidea improves the metabolic profile through expansion of adipose tissue. *Nature communications* **6**, 7433 (2015).

52. Pryce, C.R., Bettschen, D., Nanz-Bahr, N.I. & Feldon, J. Comparison of the effects of early handling and early deprivation on conditioned stimulus, context, and spatial learning and memory in adult rats. *Behav Neurosci* **117**, 883-893 (2003).

53. Spandl, J., White, D.J., Peychl, J. & Thiele, C. Live cell multicolor imaging of lipid droplets with a new dye, LD540. *Traffic* **10**, 1579-1584 (2009).

54. Meissburger, B.*, et al.* Adipogenesis and insulin sensitivity in obesity are regulated by retinoid-related orphan receptor gamma. *EMBO Mol Med* **3**, 637-651 (2011).

55. Sanchez-Gurmaches, J. & Guertin, D.A. Adipocytes arise from multiple lineages that are heterogeneously and dynamically distributed. *Nature communications* **5**, 4099 (2014).

56. Mehlem, A., Hagberg, C.E., Muhl, L., Eriksson, U. & Falkevall, A. Imaging of neutral lipids by oil red O for analyzing the metabolic status in health and disease. *Nature protocols* **8**, 1149-1154 (2013).

57. Love, M.I., Huber, W. & Anders, S. Moderated estimation of fold change and dispersion for RNA-seq data with DESeq2. *Genome Biol* **15**, 550 (2014).

58. von Meyenn, F.*, et al.* Comparative Principles of DNA Methylation Reprogramming during Human and Mouse In Vitro Primordial Germ Cell Specification. *Dev Cell* **39**, 104-115 (2016).

59. Krueger, F. & Andrews, S.R. Bismark: a flexible aligner and methylation caller for Bisulfite-Seq applications. *Bioinformatics* **27**, 1571-1572 (2011).

Figure 1

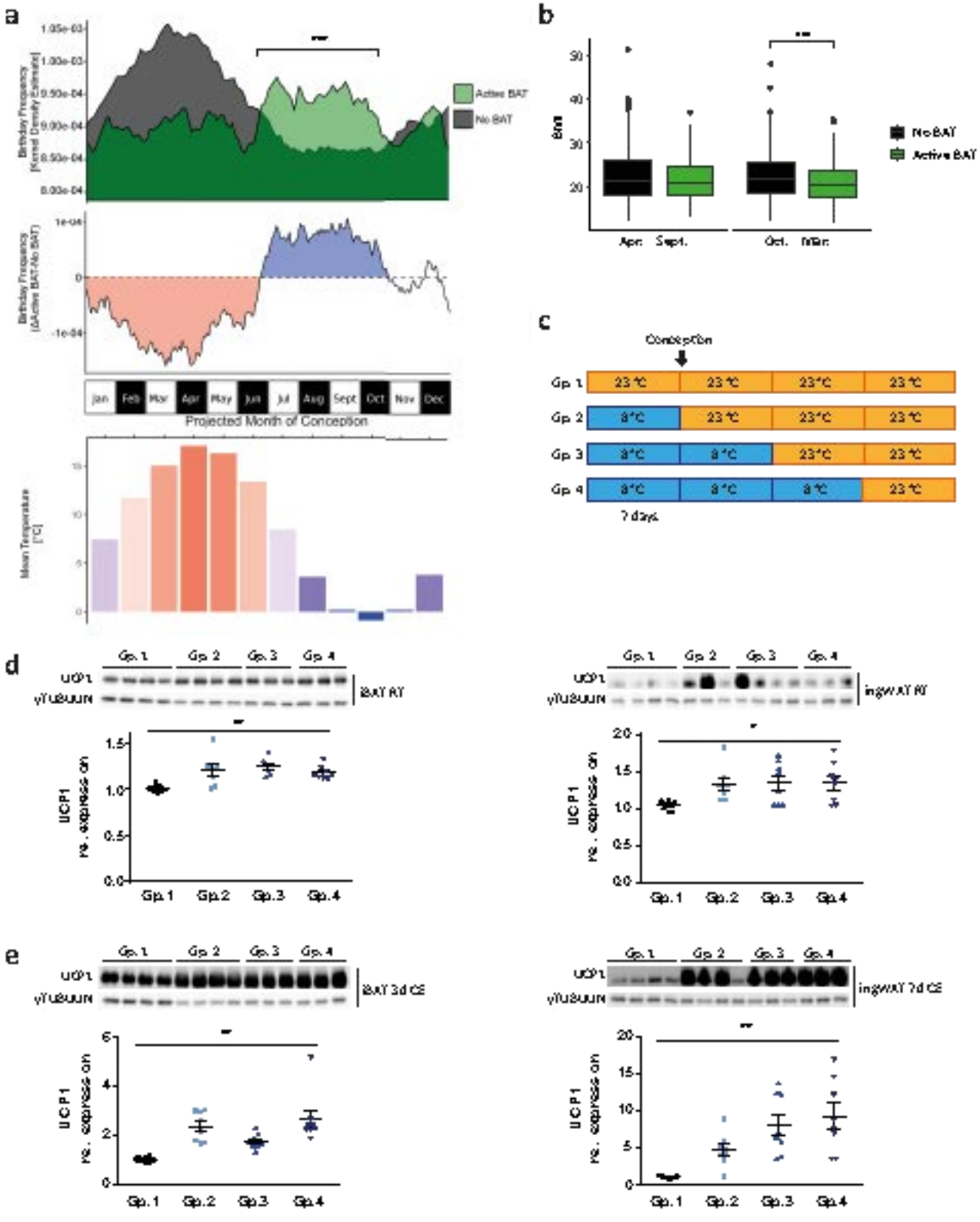
a
Active BAT
No BAT
Birthday Frequency (Kernel Density Estimate)
Birthday Frequency (ΔActive BAT-No BAT)
Jan Feb Mar Apr May Jun Jul Aug Sept Oct Nov Dec
Projected Month of Conception
Mean Temperature [°C]
b
No BAT
Active BAT
Apr. Sept. Oct. Mar.
c
Conception
Gp.1 23 °C 23 °C 23 °C 23 °C
Gp.2 8 °C 23 °C 23 °C 23 °C
Gp.3 8 °C 8 °C 23 °C 23 °C
Gp.4 8 °C 8 °C 8 °C 23 °C
7 days
d
Gp.1 Gp.2 Gp.3 Gp.4
UCP1
γTubulin
BAT RT
ingWAT RT
UCP1 rel. expression
e
BAT 3d CE
ingWAT 7d CE

Figure 2

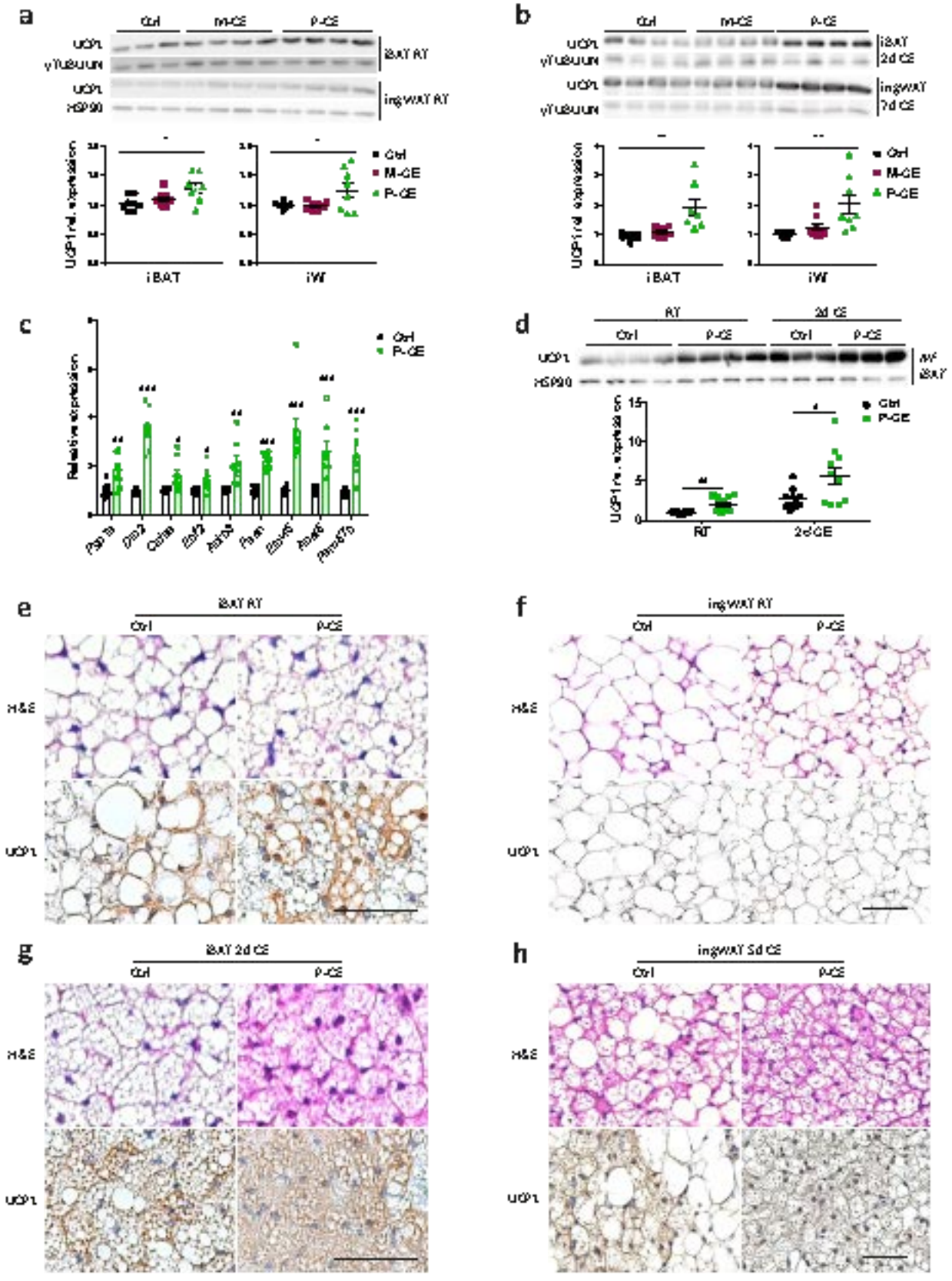
a
Ctrl
M-CE
P-CE
UCP1
vTubulin
iBAT RT
UCP1
HSP90
ingWAT RT
UCP1 rel. expression
Ctrl
M-CE
P-CE
iBAT
iW
b
Ctrl
M-CE
P-CE
UCP1
vTubulin
iBAT
2d CE
UCP1
vTubulin
ingWAT
7d CE
UCP1 rel. expression
Ctrl
M-CE
P-CE
iBAT
iW
c
Relative expression
Ctrl
P-CE
Pgc1a
Dio2
Cidea
Elvl3
Atp5i
Pparg
Elovl6
Atp6
Ppargc1b
d
RT
2d CE
Ctrl
P-CE
Ctrl
P-CE
UCP1
HSP90
iW
iBAT
UCP1 rel. expression
Ctrl
P-CE
RT
2d CE
e
iBAT RT
Ctrl
P-CE
H&E
UCP1
f
ingWAT RT
Ctrl
P-CE
H&E
UCP1
g
iBAT 2d CE
Ctrl
P-CE
H&E
UCP1
h
ingWAT 5d CE
Ctrl
P-CE
H&E
UCP1

Figure 3

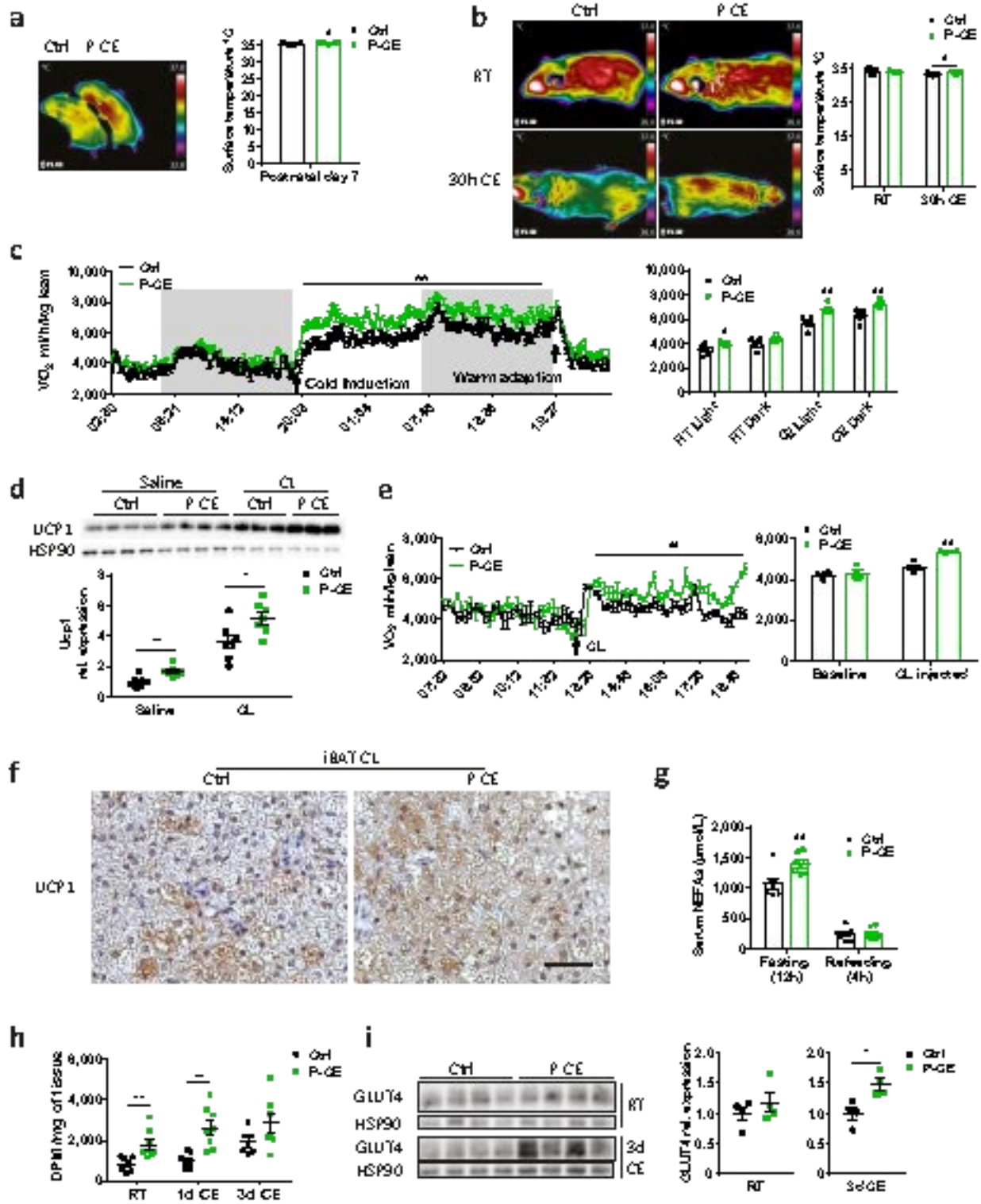
a
Ctrl
P CE
Surface temperature °C
Postnatal day 7
Ctrl
P-CE
b
Ctrl
P CE
RT
30h CE
Surface temperature °C
RT
30h CE
c
VO2 ml/h/kg lean
Cold induction
Warm adaption
RT Light
RT Dark
CE Light
CE Dark
d
Saline
CL
Ucp1
HSP90
Ucp1 rel. expression
e
GL
Baseline
GL injected
f
iBAT CL
UCP1
g
Serum NEFAs (µmol/L)
Fasting (12h)
Refeeding (4h)
h
DPM/mg of tissue
RT
1d CE
3d CE
i
GLUT4
HSP90
3d CE
GLUT4 rel. expression

Figure 4

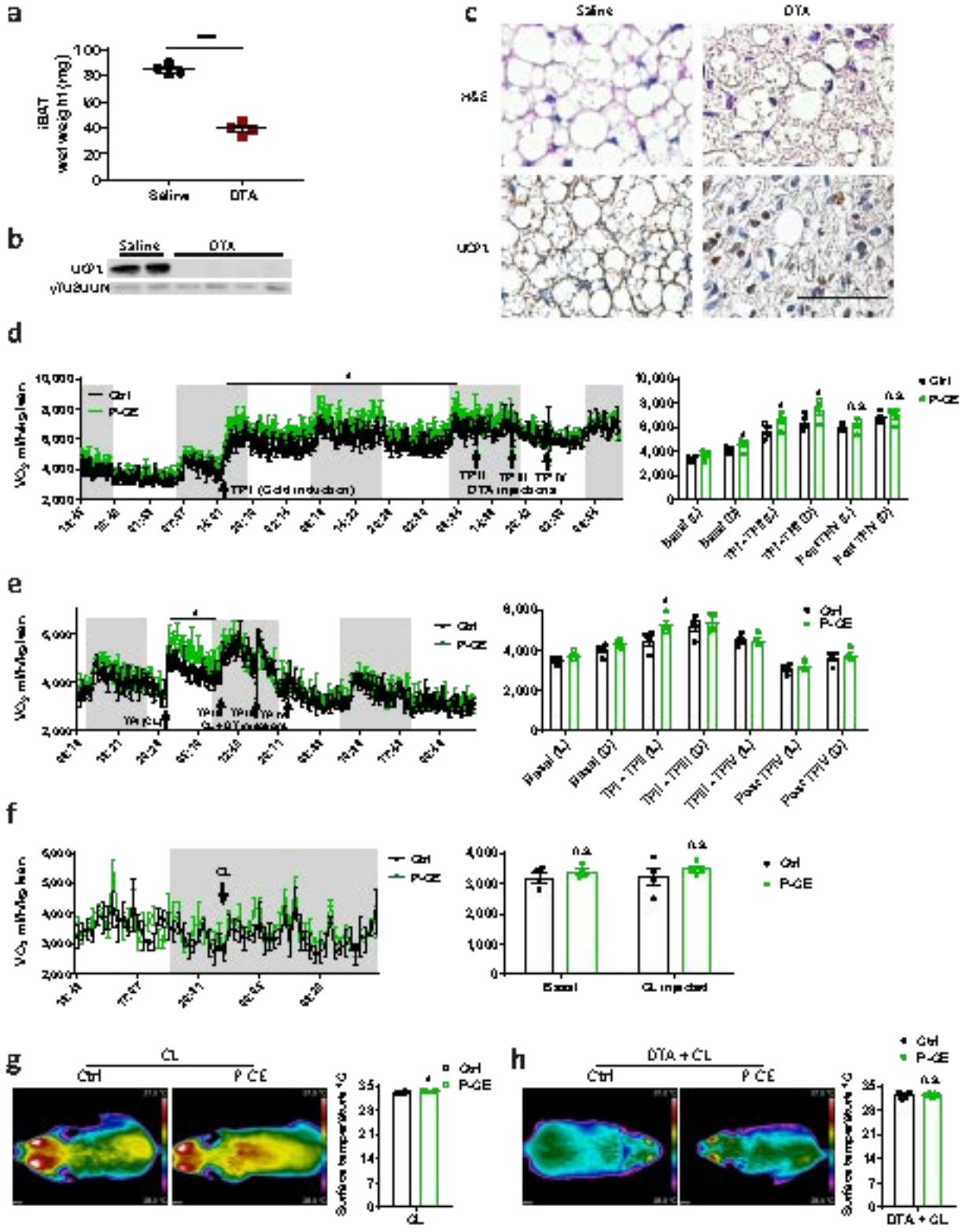
a
iBAT wet weight (mg)
Saline
DTA
b
Saline
DTA
UCP1
γ-tubulin
c
Saline
DTA
H&E
UCP1
d
Ctrl
P-CE
TPI (Cold induction)
TPII
TPIII
TPIV
DTA injections
Basal (L)
Basal (D)
TPI - TPII (L)
TPI - TPII (D)
Post TPIV (L)
Post TPIV (D)
n.s.
e
TPI (CL)
CL + DTA injections
f
CL
Basal
CL injected
g
CL
Ctrl
P-CE
Surface temperature (°C)
h
DTA + CL
Ctrl
P-CE
Surface temperature (°C)
DTA + CL

Figure 5

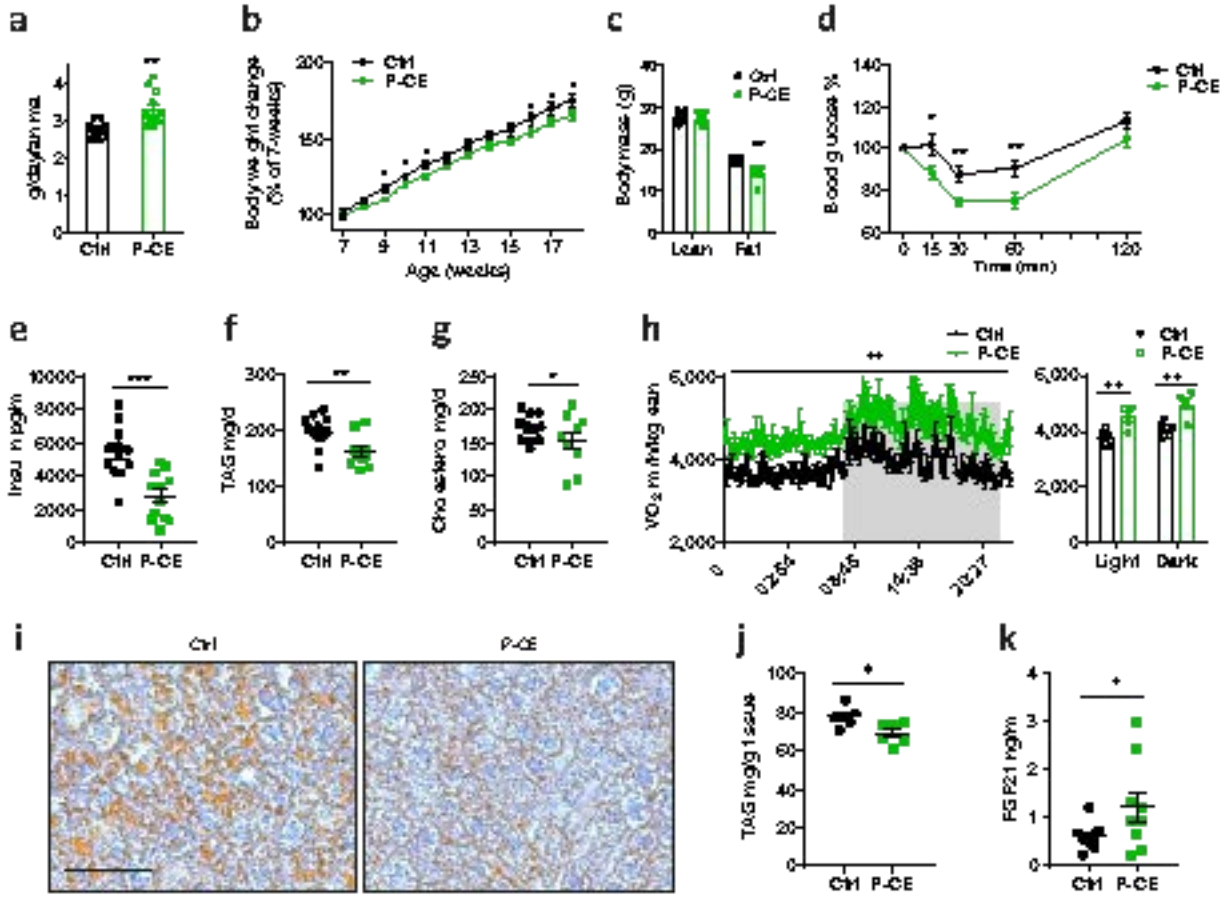

Figure 6

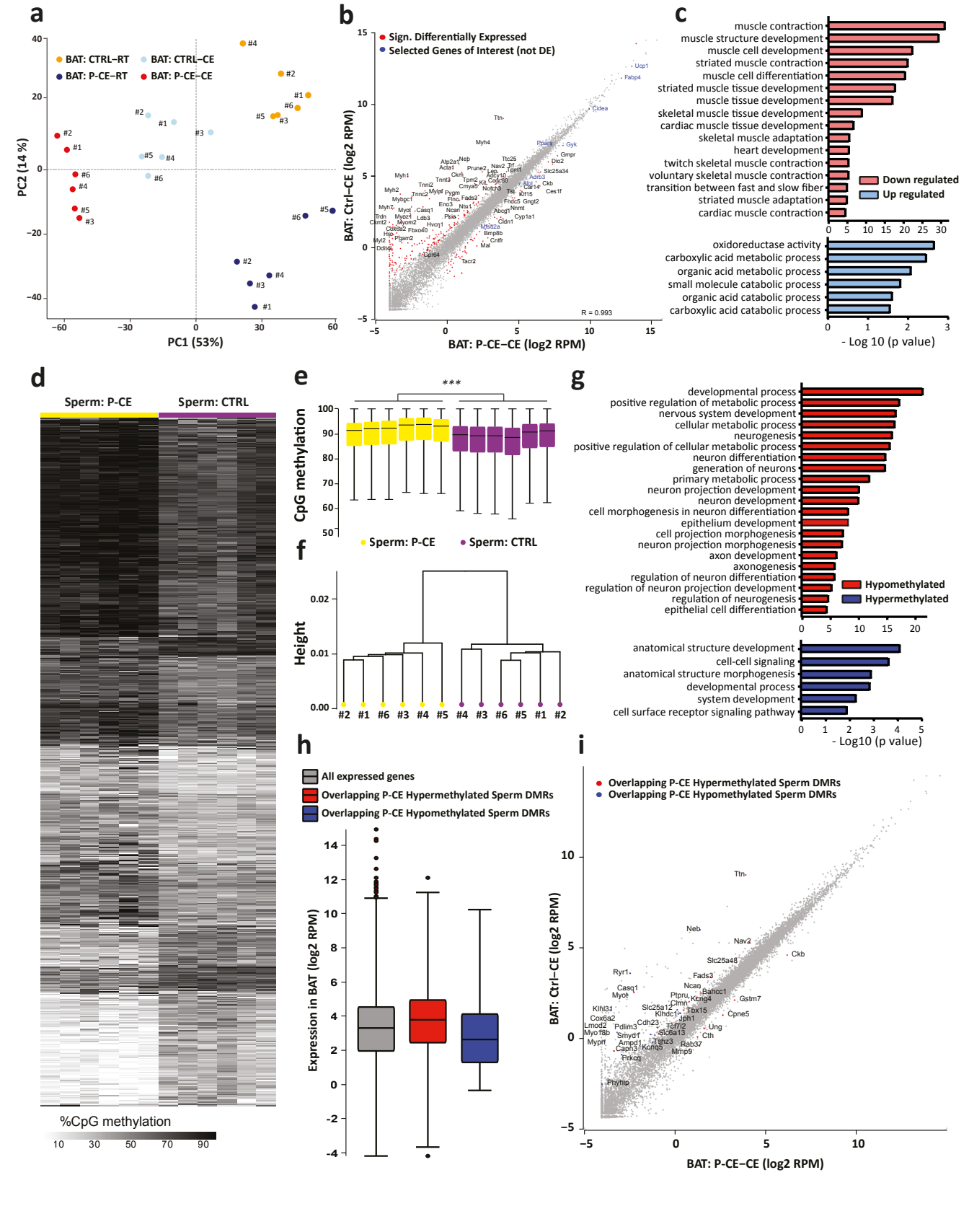
a
BAT: CTRL–RT
BAT: CTRL–CE
BAT: P-CE–RT
BAT: P-CE–CE
PC1 (53%)
PC2 (14 %)
b
Sign. Differentially Expressed
Selected Genes of Interest (not DE)
BAT: Ctrl–CE (log2 RPM)
BAT: P-CE–CE (log2 RPM)
R = 0.993
c
muscle contraction
muscle structure development
muscle cell development
striated muscle contraction
muscle cell differentiation
striated muscle tissue development
muscle tissue development
skeletal muscle tissue development
cardiac muscle tissue development
skeletal muscle adaptation
heart development
twitch skeletal muscle contraction
voluntary skeletal muscle contraction
transition between fast and slow fiber
striated muscle adaptation
cardiac muscle contraction
Down regulated
Up regulated
oxidoreductase activity
carboxylic acid metabolic process
organic acid metabolic process
small molecule catabolic process
organic acid catabolic process
carboxylic acid catabolic process
- Log 10 (p value)
d
Sperm: P-CE
Sperm: CTRL
%CpG methylation
e
***
CpG methylation
Sperm: P-CE
Sperm: CTRL
f
Height
g
developmental process
positive regulation of metabolic process
nervous system development
cellular metabolic process
neurogenesis
positive regulation of cellular metabolic process
neuron differentiation
generation of neurons
primary metabolic process
neuron projection development
neuron development
cell morphogenesis in neuron differentiation
epithelium development
cell projection morphogenesis
neuron projection morphogenesis
axon development
axonogenesis
regulation of neuron differentiation
regulation of neuron projection development
regulation of neurogenesis
epithelial cell differentiation
Hypomethylated
Hypermethylated
anatomical structure development
cell-cell signaling
anatomical structure morphogenesis
developmental process
system development
cell surface receptor signaling pathway
- Log10 (p value)
h
All expressed genes
Overlapping P-CE Hypermethylated Sperm DMRs
Overlapping P-CE Hypomethylated Sperm DMRs
Expression in BAT (log2 RPM)
i
Overlapping P-CE Hypermethylated Sperm DMRs
Overlapping P-CE Hypomethylated Sperm DMRs
BAT: Ctrl–CE (log2 RPM)
BAT: P-CE–CE (log2 RPM)